SCIENCE CHINA Materials REVIEWS

mater.scichina.com link.springer.com

Published online 28 September 2023 | https://doi.org/10.1007/s40843-023-2578-5
Sci China Mater 2023, 66(11): 4165–4181

SPECIAL TOPIC: High-performance Structural Materials

Progress of high-entropy alloys prepared using selective laser melting

Xinfang Song and Yong Zhang*

ABSTRACT **The multi-component characteristics of high-entropy alloys (HEAs) endow them with excellent performance that many traditional alloys cannot match. However, there are still some limitations in the preparation of HEAs using traditional methods. Selective laser melting (SLM) technology can achieve the precision formation of complex components through layer-by-layer deposition. It has been found that the performance advantages of HEAs can be fully utilized by combining SLM technology with HEAs. The microstructures and properties of SLM-prepared HEAs are reviewed in this study. It has been observed that due to the high-temperature gradients and high cooling rates of SLM processes, complex microstructures are usually formed in SLM-prepared HEAs, including cellular substructures, precipitates, stacking faults, and nanotwins. This study also determines that those unique microstructures bring excellent mechanical and functional properties to HEAs, indicating that the preparation of HEAs using SLM technology has major development potential. In addition, this study briefly introduces the microstructural defects and potential applications of SLM-prepared HEAs. The results obtained in this investigation provide useful guidance for the future designs of high-performance HEAs.**

Keywords: high-entropy alloys, selective laser melting, microstructure characteristics, performance characteristics, potential applications

INTRODUCTION

High-entropy alloys (HEAs) are also referred to as multi-component alloys or multi-principal element alloys. HEAs are a new type of materials with high configurational entropy that introduce "chemically disordered" structures into alloys by mixing a variety of main elements [1,2]. High configurational entropy is conducive to the random occupancy of different atoms. This makes HEAs more inclined to form simple solid solutions of face-centered cubic (FCC), body-centered cubic (BCC), or hexagonal close-packing (HCP) structures [3,4], thereby avoiding the formation of brittle intermetallic compounds [5,6]. With the development of the concept of "high entropy" in recent years, the constituent elements of HEAs have gradually expanded from the initial five-element system to four- and three-element systems. Consequently, the concept of "high entropy" has gradually expanded to "medium entropy"/"low entropy" [7]. Therefore, the term "high entropy" no longer refers to the value of entropy, but reflects the degree of chemical disorder of a certain alloy system [8]. The design concepts of multi-principal elements bring many excellent properties to HEAs and break through the performance limitations of traditional alloys, such as overcoming strength–ductility trade-offs [9,10], good soft magnetic properties [11,12], and oxidation resistance [13–15].

At present, the traditional preparation methods of HEAs mainly include arc-melting methods [11,16], powder-metallurgy methods [17–20], and magnetron-sputtering methods [21,22]. However, it has been found that the HEAs prepared by such methods usually have large numbers of metallurgical defects. For example, the HEAs prepared by arc-melting methods tend to have uneven compositions and large numbers of shrinkage cavities [23], which require complex subsequent processes to achieve excellent properties, such as forging [24,25] and rolling [26–28]. Therefore, there is an urgency to actively explore new preparation methods to achieve fast and efficient preparation of HEAs.

Additive manufacturing (AM) is a technology based on a computer-aided design (CAD) mode [23]. Metal powders or wires are utilized as raw materials, and objects are constructed by successive deposition in a layer-by-layer manner [29–31]. AM technology has high design freedom and can realize the direct formation of complex components [32,33]. AM technology has been widely used in aerospace, medical equipment, automobile manufacturing, and other fields due to those unique advantages. At present, AM technology mainly includes selective laser melting (SLM), laser melting deposition (LMD), and selective electron beam melting (SEBM). SLM is a powder bed fusion technology that can selectively melt powder bed regions with laser beams. The elevated-temperature gradients and high cooling rates during SLM processes [34] are beneficial for promoting the formation of solid solutions, thereby indicating that SLM has major development potential in preparing HEAs with highly saturated solid solutions [35]. In addition, due to its high precision and good surface quality, SLM has been widely used in the preparation of complex components [36,37]. Its schematic diagram is shown in Fig. 1a [38]. Prior to the focused laser beams commencing the scanning process, a horizontal scraper is used to scrape metal powders onto substrates in the processing chamber. Then, according to the preset data information of the current layer, high-energy laser beams selectively melt the metal powders onto the substrate. When the current layer is finished, the horizontal scraper continues to lay a new layer of metal

Beijing Advanced Innovation Center of Materials Genome Engineering, State Key Laboratory for Advanced Metals and Materials, University of Science and Technology Beijing, Beijing 100083, China
* Corresponding author (email: drzhangy@ustb.edu.cn)

powders, and the high-energy laser beams continue to selectively melt powders according to the preset data of the next layer until the entire component is manufactured. When the metal powders are in contact with the high-energy laser beams, melt pools will be instantly formed. The sizes and shapes of melt pools can be adjusted by controlling the laser processing parameters [39]. Fig. 1b shows three different types of melt pools.

The preparation methods of HEAs *via* the SLM technology have attracted increasing attention of researchers in recent years. However, there are currently few relevant research reviews available. This paper focuses on the unique microstructures and performance characteristics (including mechanical and functional properties) of HEAs prepared using the SLM technology. In addition, a brief introduction is given to the microstructural defects and potential applications of SLM-prepared HEAs, as well as a look forward to possible future development directions.

MICROSTRUCTURAL CHARACTERISTICS

SLM-prepared HEAs have very unique microstructures. In general, there are many special structures inside ultra-fine grains, such as cellular substructures, precipitates, and nanotwins [40–42]. These abundant features make the microstructures of HEAs appear to be both diverse and complex.

Grain features

The grains of SLM-prepared HEAs present typical columnar grains morphology, and those columnar grains usually grow epitaxially through fusion lines during the layer-by-layer construction processes. Some previous studies [43–45] have shown that the formation of columnar grains is related to the direction of the heat flow conduction, which is usually along the deposition direction. Generally speaking, the melting, solidification, and cooling of the powders during SLM processes are carried out quickly, resulting in elevated temperature gradients ($\sim 10^7$ K m^{-1}) inside the molten pools. In addition, during the layer-by-layer deposition processes, the deposited layers will be remelted and combined with the newly deposited layers as a whole. This results in the columnar grains throughout the molten pool lines [46,47].

The grains can effectively be refined *via* SLM, which is mainly related to the high solidification and nucleation rates during the SLM processes. As detailed in Fig. 2, Lin *et al.* [48] successfully prepared FeCoCrNi HEA using the SLM technology and obtained ultrafine columnar grains. The grains grew epitaxially along the deposition direction. In addition, it is known that the introduction of nano-ceramic phases (such as carbides and nitrides) into HEAs prepared using SLM can further refine the grains [49,50]. Li *et al.* [49] introduced 12 wt% nano-sized TiN particles into CoCrFeNiMn HEA. The results revealed that those nano-sized TiN particles were uniformly dispersed in the HEA matrix, strongly pinning the grain boundaries. A review of the statistics revealed that the average grain size was refined to less than 2 μm.

Cellular substructures

Cellular substructures are composed of many high-density dislocation networks, which are special structures commonly found in SLM-processed HEAs. During SLM processes, the powders are melted and solidified layer by layer. HEAs undergo multicycle thermal history and intense heating and cooling of micro-

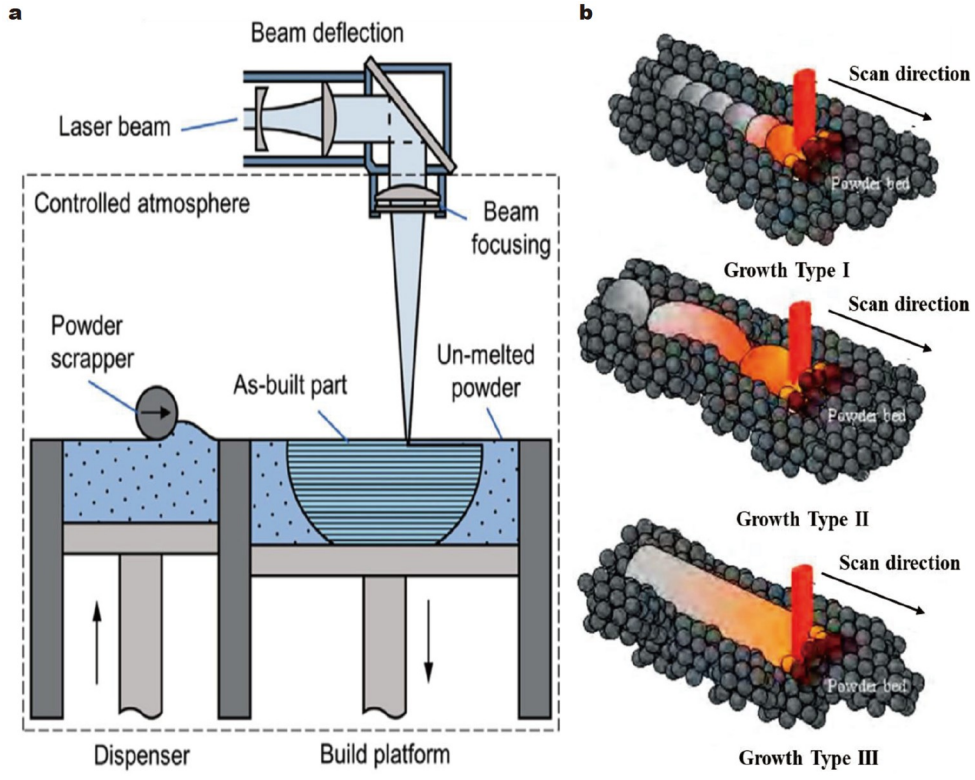

Figure 1 (a) Schematic diagram of the SLM process. Reprinted with permission from Ref. [38], Copyright 2022, Elsevier. (b) Three types of melt pools with growth type I (balled melt pool), type II (discontinuous and fragmented melt pools), and type III (continuous melt pool columns). Reprinted with permission from Ref. [39], 2018, the authors.

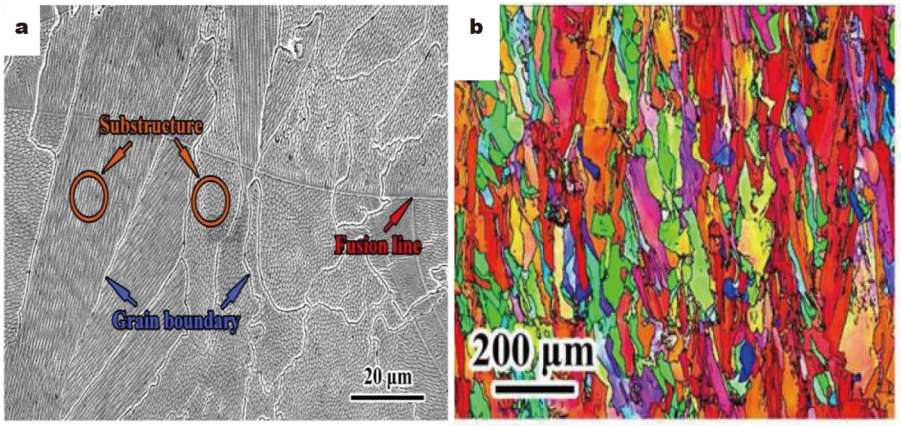

Figure 2 Micromorphology of the FeCoCrNi HEA: (a) scanning electron microscopy (SEM) image; (b) inverse pole figure. Reprinted with permission from Ref. [48], Copyright 2020, Elsevier.

regions. These repeated and non-equilibrium construction process promote the formation of tension-compression cycles inside HEAs [51], as shown in Fig. 3a, which results in the generation of high-density dislocations. Mu *et al.* [52] studied the microstructure evolutions of $Fe_{28.0}Co_{29.5}Ni_{27.5}Al_{8.5}Ti_{6.5}$ HEA prepared using SLM at different plastic strain stages (4% and 9.5%) under room-temperature conditions. As can be seen in Fig. 3b–d, the results revealed that as the strain increased from 0 to 9.5%, the cellular substructures did not undergo obvious deformation. Those findings indicated that the cellular substructures could still maintain good structural stability under high strain conditions. In addition, some studies [53] have shown that the existence of cellular substructures renders HEAs in a high-energy metastable state. After high-temperature treatments, the cellular substructures with high distortion energy almost disappear and transform into regular lattice structures with low-energy states, resulting in significant reductions in dislocation densities.

Precipitates

Nano-scale precipitates, such as intermetallic compounds or oxides, are usually *in-situ* generated in SLM-produced HEAs and uniformly distributed in the grain boundary and sub-grain boundary regions [48,54]. This is the results of the redistribution of solute atoms, which is facilitated by the abundance of high-energy state interfaces during the repeated heating-cooling cycles. Chen *et al.* [55] prepared CoCrFeMnNi HEA using SLM technology by mixing CoCrFeNi pre-alloyed powders and Mn elemental powders. It was found that the *in-situ* alloying of Mn atoms with oxygen atoms from the powders and the printing atmosphere had formed spherical Mn_2O_3 and MnO nano-oxides with a volume fraction of 7%. Luo *et al.* [36] used the SLM technology to design $AlCrCuFeNi_{3.0}$ HEA with FCC + B2 dual-phase structures. As can be seen in the TEM images in Fig. 4, the B2 phase contained abundant coherent A2 nano-scale precipitates that were mainly composed of Cr and Fe elements. In addition, similar to the traditional preparation methods, the generation of precipitates could be further promoted by appropriate heat treatments for the SLM-processed HEAs [56,57]. However, the difference is that SLM-processed HEAs only need to undergo short heat treatments due to the existence of abundant high-energy state interfaces which promote the atomic diffusion rates.

Stacking faults (SFs) and nanotwins

During SLM processes, local ultrafast heating and cooling cycles often lead to high thermal stress that can promote the formation of SFs and nanotwins. The SLM-prepared CoCrFeMnNi HEA proved that nano-twins can be formed without plastic deformation [58], and the existence of SFs was detected near nano-twins. The HRTEM images are shown in Fig. 5a, b. The results demonstrated that the low SF energy of the CoCrFeMnNi HEA, along with the rapid solidification, were conducive to the formation of SFs and nanotwins. In addition, as shown in Fig. 5c, d, the C-containing CoCrFeNi HEA prepared using SLM had both many SFs and a small number of nano-twins [59], which has rarely been reported in HEAs directly prepared using traditional processes [60,61].

MICROSTRUCTURAL DEFECTS

Some microscopic defects may exist in SLM-processed HEAs, such as pores, microcracks and residual stress, which could seriously damage the properties of HEAs and result in premature failure during service [62–64]. Therefore, minimizing the occurrences of metallurgical defects can greatly help improve performance results. Furthermore, optimizing the process parameters, such as laser powers, scanning speeds, and layer thicknesses, can help realize the control of the quality of HEAs and reduce the influencing effects of defects on performance results [65–67]. Therefore, with the goal of assisting in the preparation of high-performance HEAs, this study focuses on several typical metallurgical defects and their elimination methods.

Pores

During SLM processes, molten pools undergo rapid melting, cooling, and solidification stages, resulting in large numbers of metallurgical defects [68,69]. An abundance of pores is one of the most common metallurgical defects in SLM-fabricated HEAs [70]. High porosity will shorten the fatigue life of alloys and has major influence on mechanical properties [71,72]. The types of pores mainly include unfused pores and metallurgical pores, as shown in Fig. 6 [73]. Unfused pores are commonly caused by

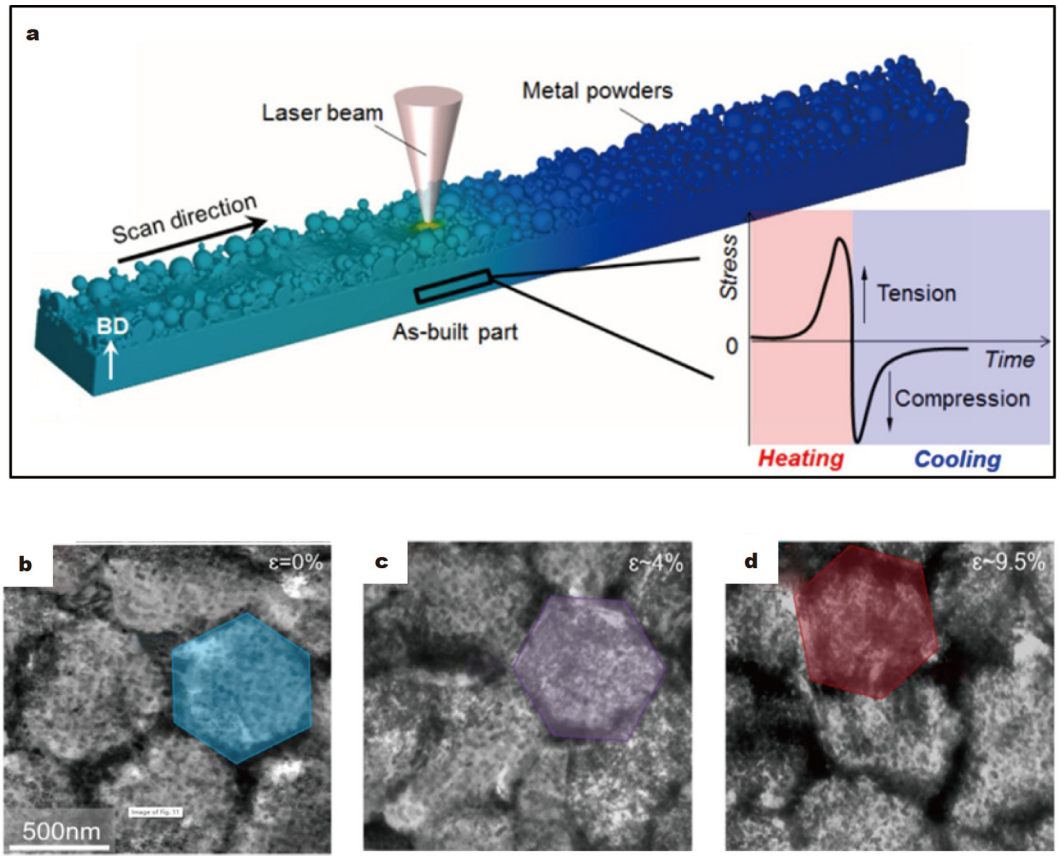

Figure 3 (a) A schematic diagram of the tension-compression cycle. Reprinted with permission from Ref. [51], Copyright 2021, Elsevier. (b–d) Transmission electron microscopy (TEM) bright-field images of the evolutions of cellular substructures of $Fe_{28.0}Co_{29.5}Ni_{27.5}Al_{8.5}Ti_{6.5}$ HEA at different plastic strain stages. Reprinted with permission from Ref. [52], Copyright 2022, Elsevier.

insufficient laser energy density, resulting in the incomplete melting of powder particles. The unfused pores are mainly distributed in the interlayer regions and display an irregular polygonal shapes, with sizes ranging up to 50 μm, or even larger [74]. The formation of metallurgical pores is due to the fact that alloy powders are hollow powders, and high energy density causes large fluctuations and instability in the molten pools, leading to spheroidization and splashing. Subsequently, gases entering the molten pools in the printing chambers will not be removed in a timely manner, resulting in the formation of circular pores inside the alloys [75,76]. The elimination of pores is a very challenging task. However, since the generation of pores is closely related to the process parameters of the SLM, optimizing the process parameters can realize the control of the porosity of HEAs. In particular, optimizing such parameters as laser powers and scanning speeds, which directly determine the sizes, shapes, and dynamics of the molten pools, can be very effective. Moreover, reasonable parameter matching can also effectively promote interlayer remelting, overlapping of adjacent molten pools, and changes in the growth directions of the grains in the molten pools, thereby reducing metallurgical defects, such as pores [77,78]. Song *et al.* [79] studied the porosity evolution of $Co_{47.5}Fe_{28.5}Ni_{19}Si_{3.4}Al_{1.6}$ HEA under different SLM processes. It was found that the laser powers had a greater effect on porosity. The porosity increased rapidly when the scanning speeds were increased from 800 to 1400 mm s^{-1}. However, the changes in the laser powers had less effect on the porosity. The comparison results indicated that the alloy produced with 200 W, 800 mm s^{-1} in SLM had the lowest porosity (0.019%). Guo *et al.* [80] obtained low-porosity $AlCoCrFeNi_{2.1}$ HEA by optimizing the process parameters. The maximum relative density reached 99.73% at the volumetric energy density (VED) of 131.87 J mm^{-3}. In addition, further follow-up treatments for SLM-processed HEAs, such as hot isostatic pressing (HIP), can also reduce the sizes and numbers of pores to a certain extent, thereby improving performance [81]. Li *et al.* [58] found large numbers of circular metallurgical pores in SLM-printed CoCrFeMnNi HEA. After HIP, the majority of the micropores closed and disappeared. It was observed that the relative density increased from 98.2% before HIP to 99.1% after HIP. In order to reduce the porosity, Gan *et al.* [82] proposed two heat treatment approaches based on annealing and HIP for SLM-printed CoCrFeNiMn HEA. The results showed that both heat treatment methods increased the density to more than 98% and achieved almost full density, with the HIP achieving the optimal microstructure and performance results.

Residual stress

Residual stress is another key defect that seriously affects the formation and service performances of HEAs. During SLM processes, the regions near the molten pools are rapidly heated at rates much higher than that of the deposited layers, resulting in local melting [83,84]. Those regions tend to expand due to the effects of heating, but are geometrically constrained by the

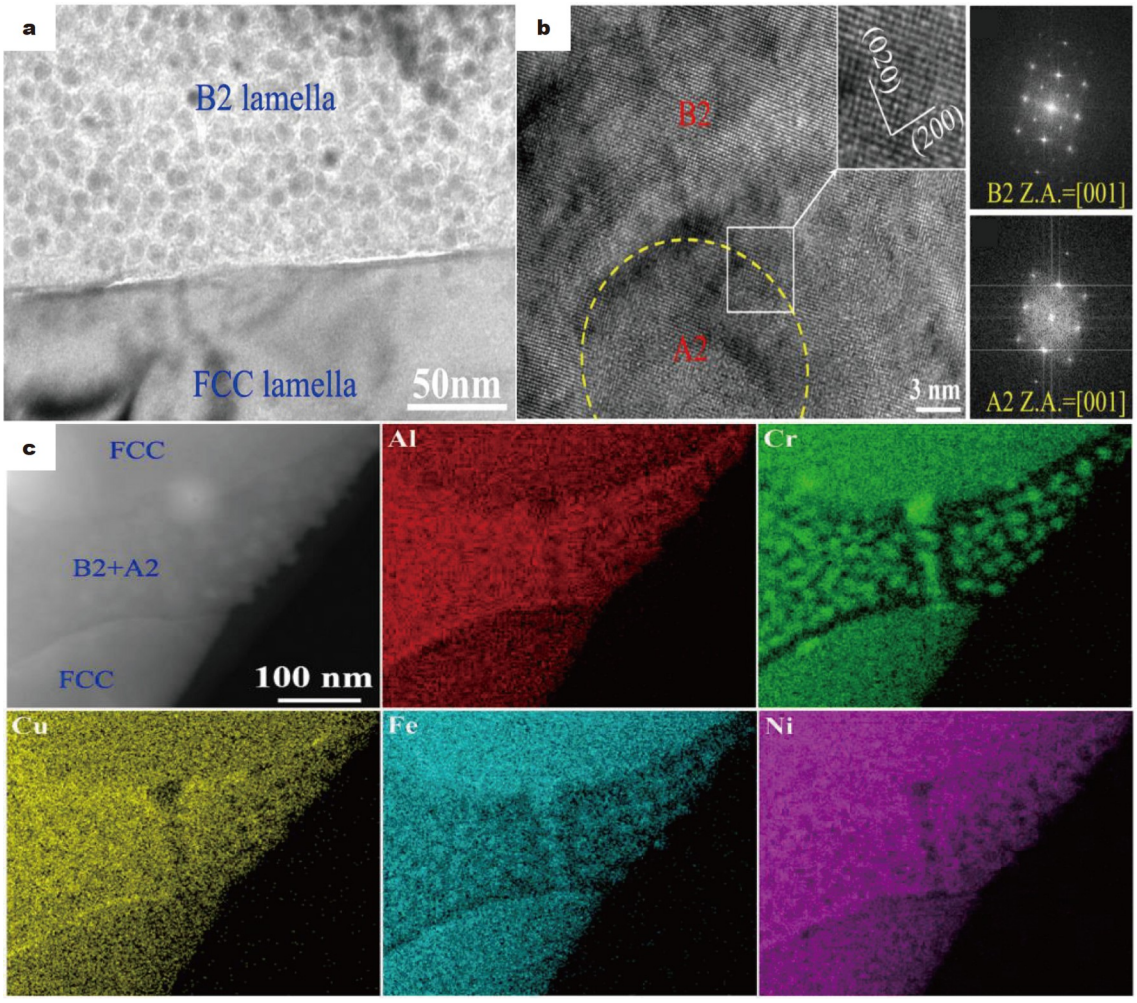

Figure 4 SLM-processed $AlCrCuFeNi_{3.0}$ HEA. (a) TEM bright-field image, showing nano-precipitates inside B2 lamella; (b) high-resolution TEM (HRTEM) image of nano-precipitate inside B2 phase and fast Fourier transform (FFT) patterns corresponding to the B2 phase and A2 nano-precipitate, respectively; (c) TEM bright-field image and corresponding TEM-X-ray energy dispersive spectroscopy (EDS) maps. Reprinted with permission from Ref. [36], Copyright 2020, Elsevier.

cooler, deposited layer regions, resulting in compressive stresses within them. However, when the molten pools cool, those regions will shrink, resulting in tensile stress conditions [85]. The repeated heating and cooling of the deposited layers give rise to alternating tensile and compressive stress inside HEAs, with residual stress accumulating. The existence of residual stress can easily lead to premature fracturing due to load instability during use. As a result, components could be destroyed and the service life of the molded components shortened [86,87]. Therefore, in order to avoid premature fracturing, the generation of residual stress should be controlled and reduced as much as possible.

Currently, the optimization of the process parameters of SLM can effectively reduce the residual stress of HEAs. Gu *et al.* [88] examined the residual stress in VNbMoTaW samples prepared using different laser scanning speeds. The results showed that the tensile residual stress was the highest when the laser scanning speed was 400 mm s^{-1}, reaching 380 MPa. Then, as the scanning speed increased, the dissipated heat in the deposited layers decreased, resulting in reductions in the temperature gradients and relative decreases in the residual stress. When the laser scanning speeds were further increased to 600 and 800 mm s^{-1}, the extracted values of the surface residual stress decreased to 280 and 210 MPa, respectively. Wang *et al.* [89] analyzed the distribution patterns of residual stress in SLM-printed AlCoCrCuFeNi HEAs *via* electron back scatter diffraction (EBSD). It was found that the residual stress of all the examined samples exhibited uneven distribution patterns with a maximum residual stress of 500 MPa. The larger the volumetric energy density, the more obvious the inhomogeneity of the distribution of the residual stress. In addition, further annealing processes for SLM-printed HEAs can also effectively release the residual stress generated during SLM processes. In order to reduce residual stress in SLM-printed FeCoCrNi HEA, Lin *et al.* [90] studied the effect of annealing temperature on residual stress by heat treating the alloy at different temperatures. It was found that the rapid solidification and cooling during SLM processes caused large residual stress of 323 ± 15.23 MPa in the sample. However, after annealing, the residual stress decreased. The higher the annealing temperature, the more obvious residual stress decreased, as shown in the Fig. 7. When the annealing temperatures were higher than 1173 K, the residual stress dropped below 200 MPa. In the studies conducted by Zhang *et al.* [91], part of the residual stress was also successfully released

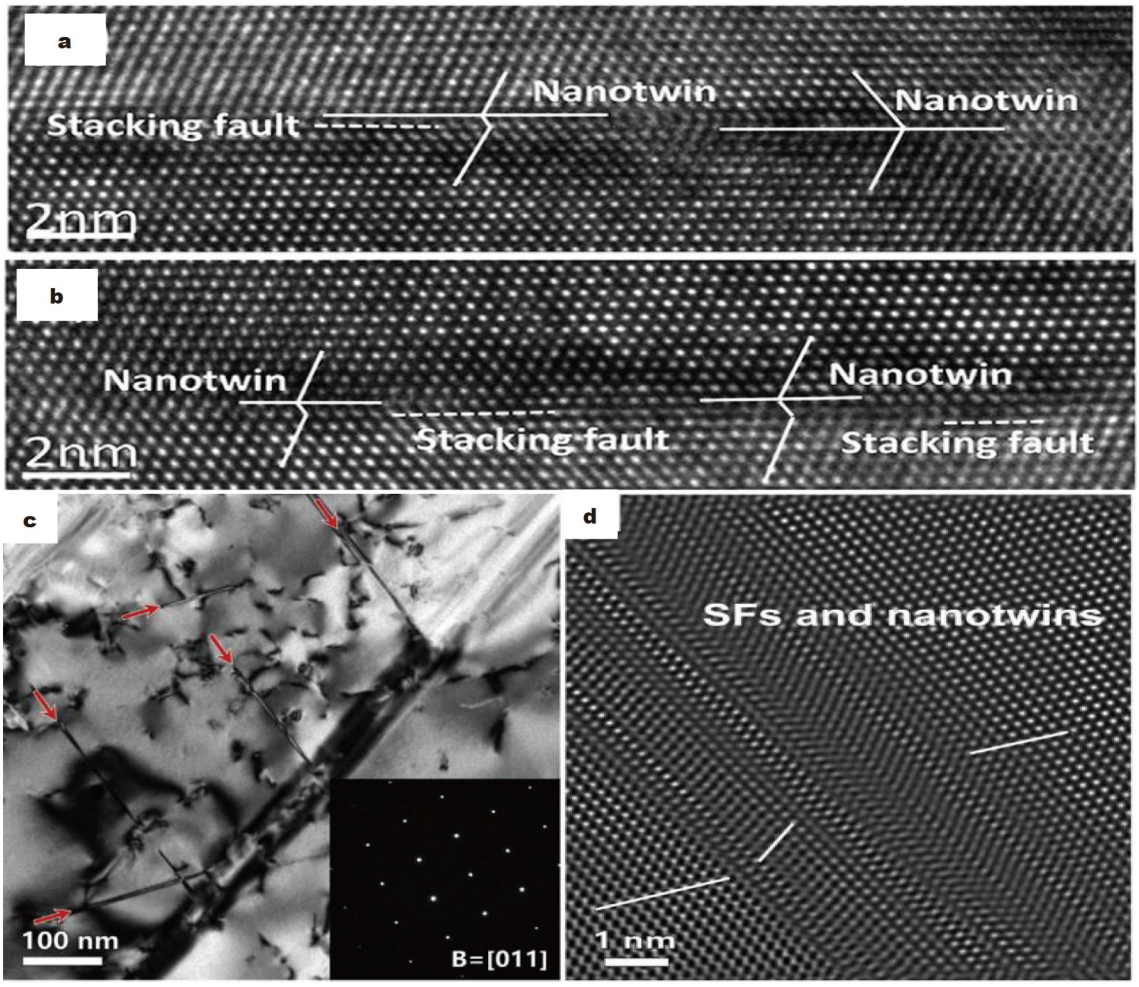

Figure 5 (a, b) HRTEM of the SLM-processed CoCrFeMnNi HEA, showing the nanotwins coupled with SFs. Reprinted with permission from Ref. [58], Copyright 2018, Elsevier. (c, d) TEM bright-field image and HRTEM of the SLM-processed C-containing CoCrFeNi HEA, respectively, showing nanotwins and SF structures (the red arrows represent SFs). The inset is the corresponding SAED pattern. Reprinted with permission from Ref. [59], Copyright 2018, Elsevier.

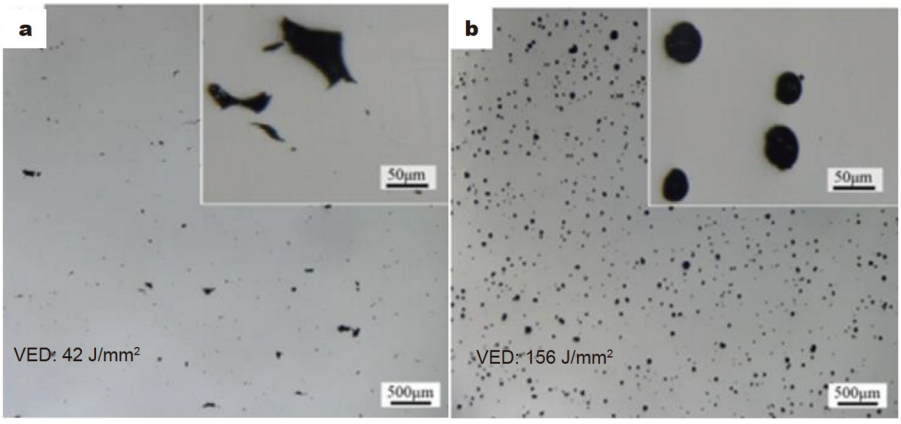

Figure 6 (a) Unfused pores; (b) metallurgical pores. Reprinted with permission from Ref. [73], Copyright 2022, Elsevier.

after heat treatments at 900 and 1000°C for SLM-printed AlCoCuFeNi HEAs.

Cracks

The presence of residual stress tends to cause microcracks in the HEAs. Microcracks are the most common and destructive defects that occur during the formation processes of SLM, which has a fatal impact on components [92–94]. Once cracks occur in components, they can only be scrapped. Previous studies [95–97] have shown that the cracks generated during SLM processes

mainly occur during the repeated heating, melting, and cooling stages of the deposited layers. When internal thermal stress is generated during the cooling stage, internal cracks can easily be induced [98–100].

Microcracks can be eliminated by reasonably adjusting the composition of HEAs. Luo *et al.* [36] promoted the transformation of the alloys from the BCC (B2) phase to the FCC phase by increasing the Ni content in $AlCrCuFeNi_x$ ($2.0 \leq x \leq 3.0$) HEAs, thereby improving the formability of the as-built $AlCrCuFeNi_x$ ($2.0 \leq x \leq 3.0$) HEAs. The microstructures of the alloys were observed, and it was found that the number of cracks decreased significantly with the increase of Ni content. Only a few micro-cracks appeared in $AlCrCuFeNi_{2.75}$ HEA. Finally, when x increased to 3.0, the micro-cracks were completely eliminated. Scanning strategies can effectively regulate grain morphology, texture, and the distribution of residual stress to control the density and morphology of cracks. In the studies conducted by Zhang *et al.* [101], three scanning strategies of 0-scan, 67-scan, and 90-scan were adopted to prepare CoCrFeMnNi HEA. The influencing effects of the scanning strategies on crack formation, as well as the formation mechanism of the cracks during the SLM processes, were systematically revealed. The results indicated that the 0-scan strategy exhibited the largest crack density, while the 67-scan strategy showed the least. The cracks formed at right-angle-shaped high angle grain boundaries (HAGBs) without elemental segregation or precipitate. The upper parts of the cracks exhibited features of hot cracking. Meanwhile, the lower parts of the cracks were more likely to be formed by the propagation of the upper parts in solid states during thermal shrinking and contraction. Sun *et al.* [102] used two different scanning strategies (chessboard and stripe/bi-directional) to reduce cracks. As can be clearly seen in Fig. 8, with the same scanning parameters but different scanning strategies, the number of cracks in the stripe sample was fewer

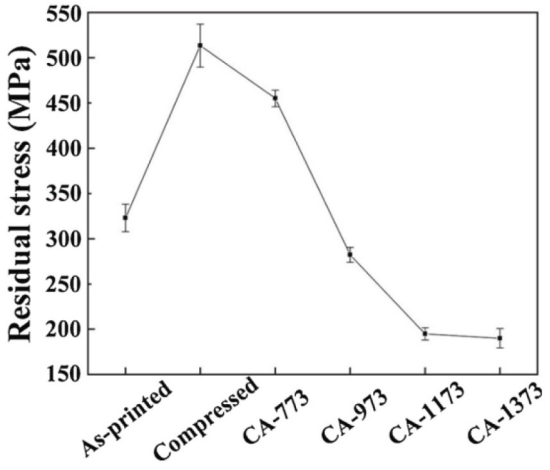

Figure 7 Variation in the residual stress on the upper surface. CA-773, CA-973, CA-1173, and CA-1373 indicated that SLM-printed FeCoCrNi HEA was annealed at 773, 973, 1173, or 1373 K for 2 h, respectively. Reprinted with permission from Ref. [90], Copyright 2020, Elsevier.

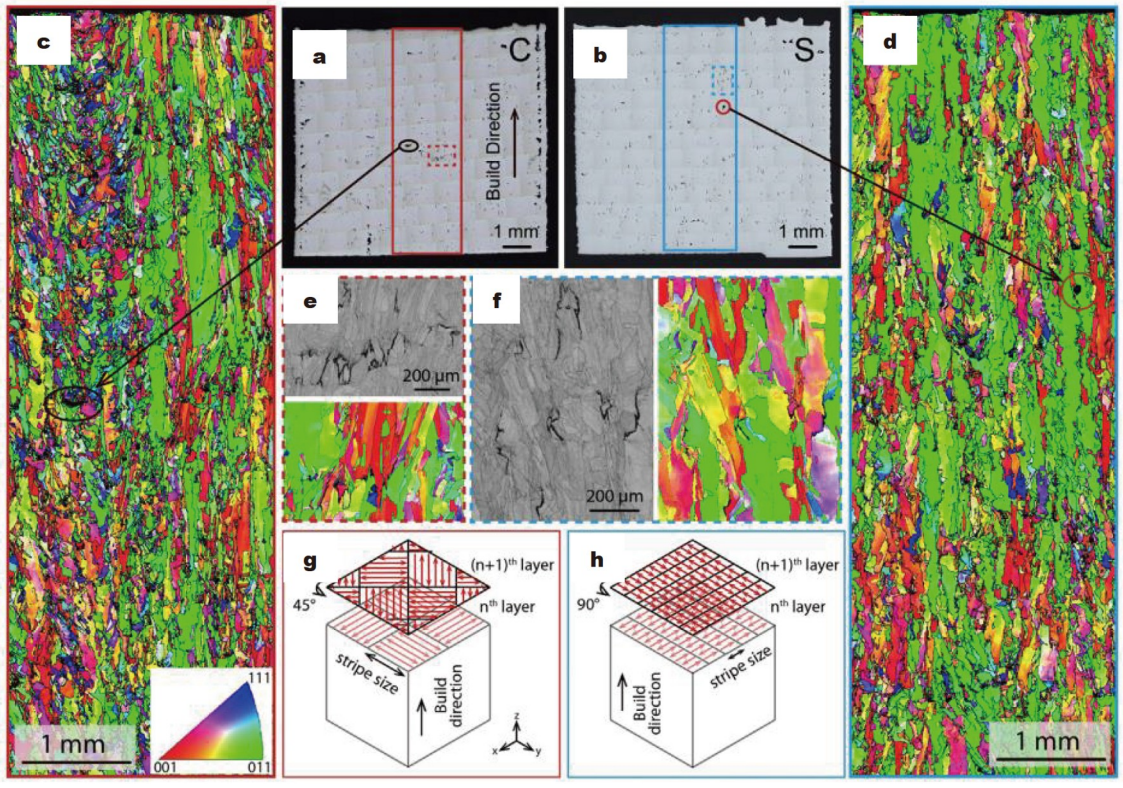

Figure 8 Optical microscopy images of SLM-built CoCrFeNi with (a) chessboard (denoted as C) and (b) stripe (denoted as S) scanning strategies. EBSD inverse pole figure (IPF) color maps with respect to the build direction of the selected areas for (c) C sample and (d) S sample. Lack-of-fusion cracks and spherical pores are highlighted in black and red circles, respectively. (e, f) Enlarged EBSD band contrast images and IPF color maps showing intergranular cracks within C and S samples, respectively. (g, h) Schematics of the chessboard and stripe scanning strategies for SLM process, respectively. Reprinted with permission from Ref. [102], Copyright 2019, Elsevier.

compared with the chessboard sample. Also, the distribution pattern of the cracks in the stripe sample was more random, which is a common phenomenon for SLM-fabricated parts. However, it was noted that the cracks in the chessboard sample aligned themselves along the build direction. Heat treatments can relieve thermal residual stress, which also helps reduce the chances of cracking. Due to the high residual stress in the as-printed CoCrFeMnNi HEA, in order to prevent cracking during the cold rolling process, Miao *et al.* [103] annealed samples at 673 K for 2 h before cold rolling. As a result, the residual stress was almost completely eliminated. Furthermore, no cracks appeared during subsequent processing. It has also been determined that preheating substrate can reduce the temperature gradients between the printed layers and the deposited layers, which can also reduce cracking.

PERFORMANCE CHARACTERISTICS

Mechanical properties

The unique microstructures shaped by SLM technology bring excellent mechanical properties to HEAs. The equiatomic FeCoCrNi HEA with a single FCC structure was the earliest SLM-processed HEAs [104]. The performance results confirmed that SLM technology has great development potential for the preparation of HEAs. The yield strength was 600 MPa, approximately three times higher than that of the cast FeCoCrNi HEA, and could be maintained at 32% of its excellent tensile plasticity. In addition, $AlCoCrFeNi_{2.1}$ HEA with FCC + B2 dual-phase structures was prepared using SLM and ultrafine eutectic lamellae (300–500 nm) were obtained [105]. The strength and ductility of the alloy were simultaneously improved. The yield strength was 1040 MPa, and the ultimate tensile strength was 1220 MPa, with an elongation of ~24%. This was significantly higher than that of the as-cast alloy with yield strength of 595 MPa, ultimate tensile strength of 1168 MPa, and total elongation of 15.8%, respectively.

Heat treatments are also effective methods for improving the mechanical properties of SLM-produced HEAs. The precipitation-strengthened $(FeCoNi)_{86}Al_7Ti_7$ HEA prepared using the SLM technology was aged at 500 and 780°C for 2 h, respectively [106]. The results showed that the coherent L12 nano-precipitates produced by the aging treatments contributed to the yield strength of the alloy increasing from an initial 710 MPa to 934 and 1203 MPa, respectively. The results confirmed that this process was an effective strengthening method for SLM-processed HEAs. However, high temperatures can also destroy the unique microstructures of HEAs prepared *via* SLM, resulting in a decreased strength [57]. Therefore, the heat treatments temperatures should not be too high.

In addition, it has been discovered that the introduction of nano-ceramic phases into SLM-processed HEAs (such as carbides and nitrides) can further enhance the strength of HEAs. Chen *et al.* [107] obtained mixed powders by the mechanical ball milling of CoCrFeMnNi prealloyed powders and 1 wt% nano-TiC particles. Then, they successfully manufactured nano-TiC reinforced CoCrFeMnNi HEA composites using SLM processes, as shown in Fig. 9. These TiC particles were uniformly distributed in the grain boundaries and within the grains, effectively hindering dislocation movement and promoting the alloy to exhibit excellent mechanical properties. For example, the yield strength was 779 MPa, tensile strength was 940 MPa, and elongation was 30%. After introducing 5 wt% NbC nanoparticles into the SLM-processed CoCrFeMnNi HEA, NbC precipitates were formed at the cell boundaries, thereby exhibiting high thermal stability [108]. Similarly, 12 wt% nano-TiN_P-reinforced CoCrFeMnNi HEA composites obtained ultra-fine grains with average grain sizes of less than 2 μm, giving the alloy both high mechanical strength and good sliding-wear resistance [49].

Functional performances

Magnetic properties

Soft-magnetic materials with high saturation magnetization M_S (or saturation induction intension B_S) and low coercivity H_C have been widely applied in electronic devices, rotating electrical machines, and wind turbines [109]. Traditional soft magnetic materials (such as Fe-Si alloys and Permalloy) have excellent soft magnetic properties, but their poor mechanical properties limit their application potential under mechanically highly loaded conditions [110–112]. Therefore, in many engineering applications, advanced soft magnetic materials not only require excellent soft magnetic properties, but also high strength and good ductility. Since HEAs contain many ferromagnetic elements (Fe, Co, and Ni), they generally exhibit excellent soft magnetic properties [12,113,114]. Some previous studies have shown [115,116] that SLM technology has major influencing effects on the microstructures, and also the magnetic and mechanical behaviors of soft magnetic HEAs. For example, it has been found that when compared with their conventionally processed counterparts, SLM-fabricated soft-magnetic HEAs often exhibit poor soft-magnetic properties. This is mainly caused by the pinning of magnetic domains *via* defects that are generated during SLM processes, such as holes, internal stress, and substructure interfaces [117,118]. However, as shown in Fig. 10, it was interesting to note that Song *et al.* [79] successfully prepared $Co_{47.5}Fe_{28.5}Ni_{19}Si_{3.4}Al_{1.6}$ HEA with excellent mechanical and soft magnetic properties by optimizing the process parameters of SLM. By comparison, the sample produced with 200 W, 800 mm s^{-1} in SLM had achieved optimum comprehensive properties, with B_S, H_C, and μ_{max} (maximum permeability) of 1.479 T, 188.3 A m^{-1}, and 1171.8, respectively. The tensile yield strength and elongation were 417.0 MPa and 33.9%, respectively. Furthermore, CoFeNi alloy prepared using SLM also exhibited a good combination of soft magnetic and mechanical properties [119]. The saturation magnetization and coercivity were observed to be the same as those of conventional cast and thermo-mechanically processed samples. In addition, the SLM-processed CoFeNi alloy had higher yield strength and slightly lower ductility than conventionally processed alloys.

Corrosion resistance

The majority of the constituent elements of HEAs contain one or more corrosion-resistant elements (such as Al, Cr, and Mo) that can improve the corrosion resistance of the HEAs [120,121]. Relevant research results have shown that SLM-processed HEAs have better corrosion resistance. It was found that higher solidification rates can promote the SLM-processed CoCrFeNiTi-based HEAs to form non-segregation, fine, and uniform microstructures [122], thereby obtaining excellent tensile properties, including yield strength of 773.0 MPa, ultimate tensile strength of 1178.0 MPa, elongation of 25.8%, and high pitting potential (0.88 ± 0.03 V *versus* Ag/AgCl in a 3.5% NaCl solution

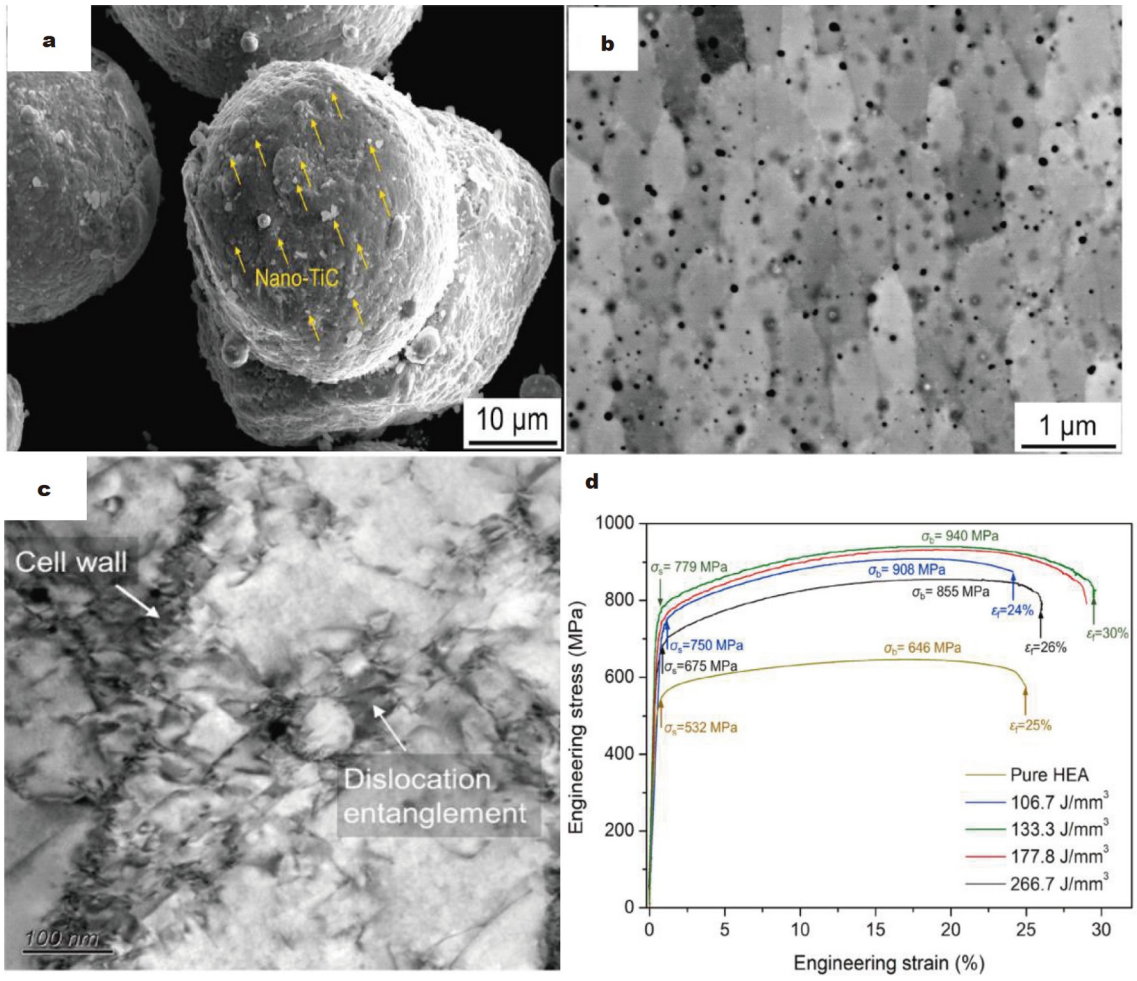

Figure 9 Nano-TiC (1 wt%)-reinforced CoCrFeMnNi HEA composites. (a) SEM image of the mixed powders, showing the distribution of nano-TiC particles on the surface of CoCrFeMnNi HEA powders; (b) SEM image of composites, showing inter-crystalline and intra-crystalline precipitates; (c) TEM bright-field image of composites, showing dislocation tangle around nano-TiC particles; (d) engineering stress-strain curves at different energy densities. Reprinted with permission from Ref. [107], Copyright 2022, Elsevier.

at 353 K), as detailed in Fig. 11. Similarly, the potentiodynamic results of $Fe_{38.5}Mn_{20}Co_{20}Cr_{15}Si_5Cu_{1.5}$ HEA prepared using SLM [123] revealed that $Fe_{38.5}Mn_{20}Co_{20}Cr_{15}Si_5Cu_{1.5}$ HEA had a combination of good strength-ductility synergy and higher passivation tendencies.

Oxidation resistance

In high-temperature environments, excellent oxidation resistance can maintain HEAs with stable mechanical properties. At present, SLM-processed HEAs also exhibit excellent oxidation resistance potential [124]. Jia *et al.* [125] examined the high-temperature oxidation behaviors of CoCrFeMnNi HEA prepared using SLM at a temperature range of between 800 and 1000°C. It was found that there were three layers of oxide scale at all temperatures. In the range of 800 to 1000°C, the inner oxide layer was Cr_2O_3, and the intermediate layer was composed of Cr-oxides and Mn-oxides. The outer oxide layer was mainly Mn_2O_3 at 800 to 900°C and Mn_3O_4 at 1000°C. For the as-built sample, the molten pool boundaries were preferentially oxidized at 1000°C due to the fast diffusion of the Mn and Cr elements. Fortunately, subsequent annealing treatments could suppress this preferential oxidation behavior and improve oxidation resistance. Refractory HEAs usually exhibit excellent high-temperature oxidation resistance since they contain abundant high-melting point elements. Due to those advantages, they are expected to become a new generation of high-temperature materials. Chen *et al.* [126] used SLM to prepare WMoTaNbV- and TiC/WMoTaNbV-based alloys. It was found that $Ta_{16}W_{18}O_{94}$ and $Nb_{14}W_3O_{47}$ ternary oxidation products were formed inside the WMoTaNbV-based alloy after the two alloys were oxidized at the high temperature of 600°C for a long period of time. In addition, after TiC particles were added, TiO_2 and $Ti_2Nb_{10}O_{29}$ oxidation products were further generated, which was of major benefit for improving the oxidation resistance of the alloy.

APPLICATIONS OF SLM-PREPARED HEAs

Coating applications

The excellent mechanical and functional properties of HEAs indicate that they have major development potential in the preparation of surface coatings and improvements in the wear resistance, corrosion resistance, and oxidation resistance of substrate surfaces. At present, there are many methods to pre-

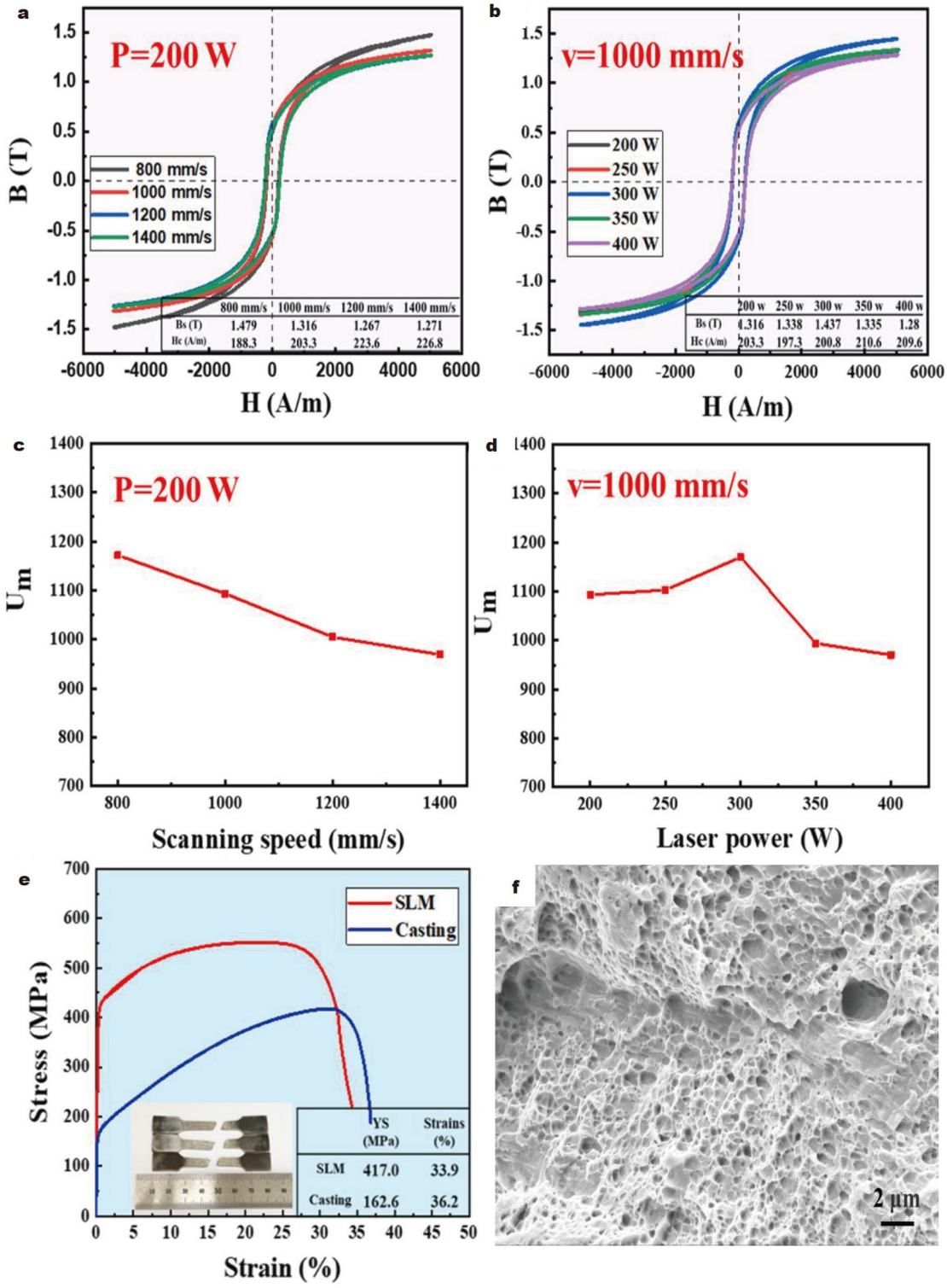

Figure 10 Hysteresis loops of $Co_{47.5}Fe_{28.5}Ni_{19}Si_{3.4}Al_{1.6}$ HEA at (a, c) 200 W, 800–1400 mm s^{-1} and (b, d) 1000 mm s^{-1}, 200–400 W; (e) engineering tensile stress-strain curves of the SLM sample with 200 W, 800 mm s^{-1} and cast sample; (f) tensile fracture micromorphology of the sample with 200 W, 800 mm s^{-1} in laser powder bed fusion (LPBF). Reprinted with permission from Ref. [79], Copyright 2023, Elsevier.

pare HEAs coatings, such as thermal spraying, cold spraying, and plasma spraying. However, the metallurgical adhesion between HEAs coatings prepared by those methods and substrates tends to be poor, and large numbers of defects may occur [127,128]. Due to the high temperature gradients and cooling rates, laser cladding (including SLM and direct laser deposition) can achieve good metallurgical bonds between HEAs coating and substrate interfaces. However, at present, direct laser deposition is mainly used to prepare HEAs coatings, and there has been less research conducting regarding SLM technology.

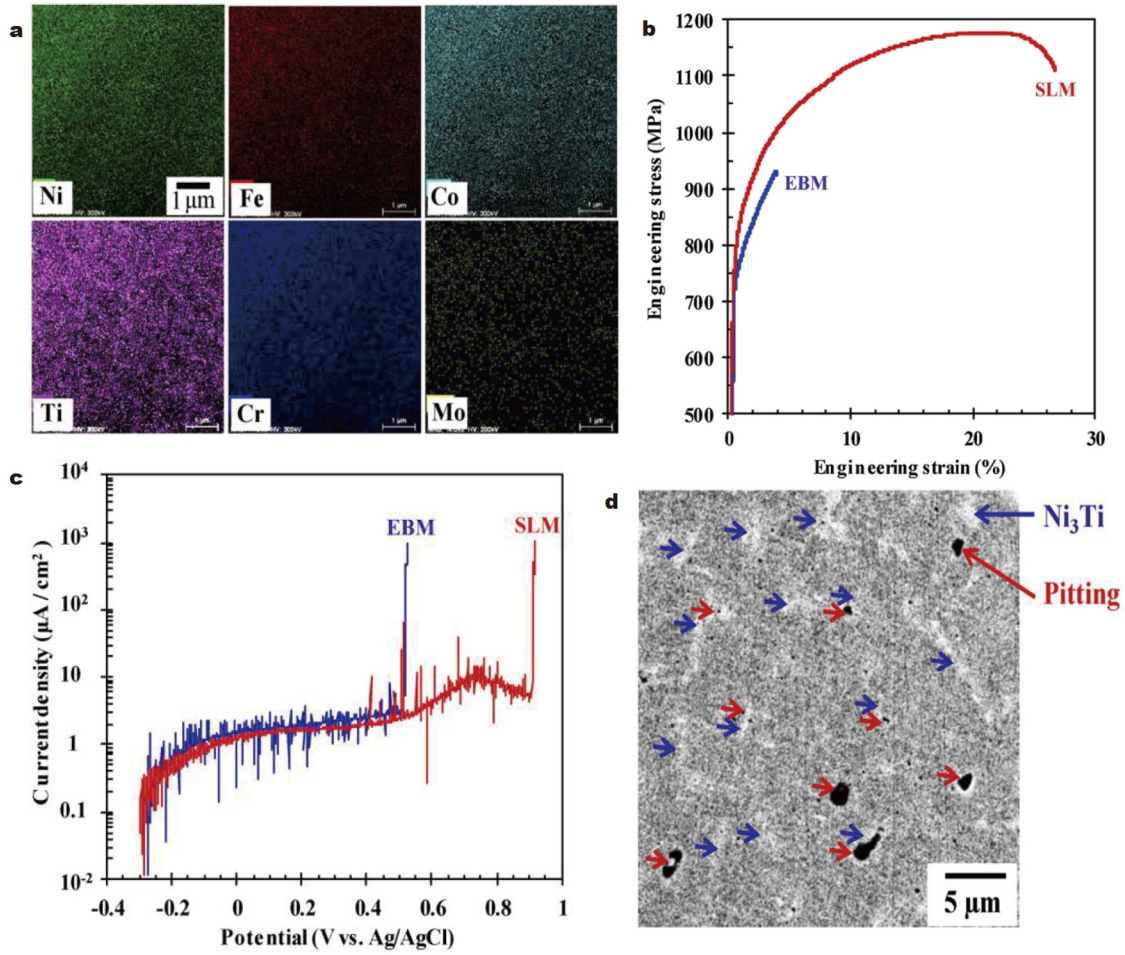

Figure 11 CoCrFeNiTi-based HEA. (a) Scanning TEM (STEM)-EDS maps of SLM-produced specimen; (b) tensile stress-strain curves of the as-built SLM and EBM specimens at room temperature; (c) representative potentiodynamic polarization curves of the as-built SLM and EBM specimens in 3.5% NaCl solution at 353 K; (d) SEM image of the SLM specimen after potentiodynamic polarization measurements in 3.5% NaCl solution at 353 K. Reprinted with permission from Ref. [122], Copyright 2019, Elsevier.

For the purpose of improving the surface properties of Q235 carbon steel, Li *et al.* [129] prepared CrFeMoNiTi$(WC)_{0.3}$ HEA composite coating *via* SLM and then studied its wear resistance and corrosion resistance. The results revealed that the WC particles and BCC phase played load-bearing roles during the friction processes and lowered the wear loss of the composite coating. The anodic protection produced by the corrosion-resistant WC particles and BCC phase also greatly improved the NaCl corrosion resistance of the composite coating. In addition, the high-temperature oxidation behaviors of the refractory $NiSi_{0.5}CrCoMoNb_{0.75}$ HEA coatings prepared using laser cladding technology were investigated [130]. It was observed that after the coating was oxidized in air at high temperatures, it formed a unique oxide layer, as shown in Fig. 12. Then, following further elemental analysis, it was demonstrated that the oxide layer was composed of $Ni_3(VO_4)_2$, Ni_3TiO_5, $NiCrO_3$, $CoCr_2O_4$, and $Nb_{0.6}Cr_{0.4}O_2$.

Applications in the manufacture of complex components

Without any additional traditional molds and machining, SLM technology is able to produce components with various complex shapes by virtue of its high dimensional accuracy and high degree of design freedom. Ren *et al.* [131] prepared three representative engineering components of $AlCoCrFeNi_{2.1}$ HEA using SLM, including a heatsink fan, an octet-truss microlattice and a gear, which demonstrated the excellent printability of $AlCoCrFeNi_{2.1}$ HEA. In addition, Zhou *et al.* [34] manufactured a small turbine blade with a bright surface and no obvious macroscopic defects through SLM (Fig. 13), verifying the feasibility of fabricating large and complex components of $Al_{0.5}FeCoCrNi$ HEA *via* SLM. Such achievements have inestimable economic benefits and strategic significance for the manufacturing development of precision components in the future.

In addition, with further improvements in the industry requirements for the comprehensive performance results of products, the concept of "lightweight" has begun to emerge [132–134]. However, the traditional preparation technologies of HEAs encounter difficulties when processing the interiors of integrated components, which limits the potential of HEAs to exploit lightweight and complex structural component advantages [135,136]. Fortunately, SLM technology has broken through the limitations of traditional technologies. Its high precision and enhanced design freedom can introduce complex

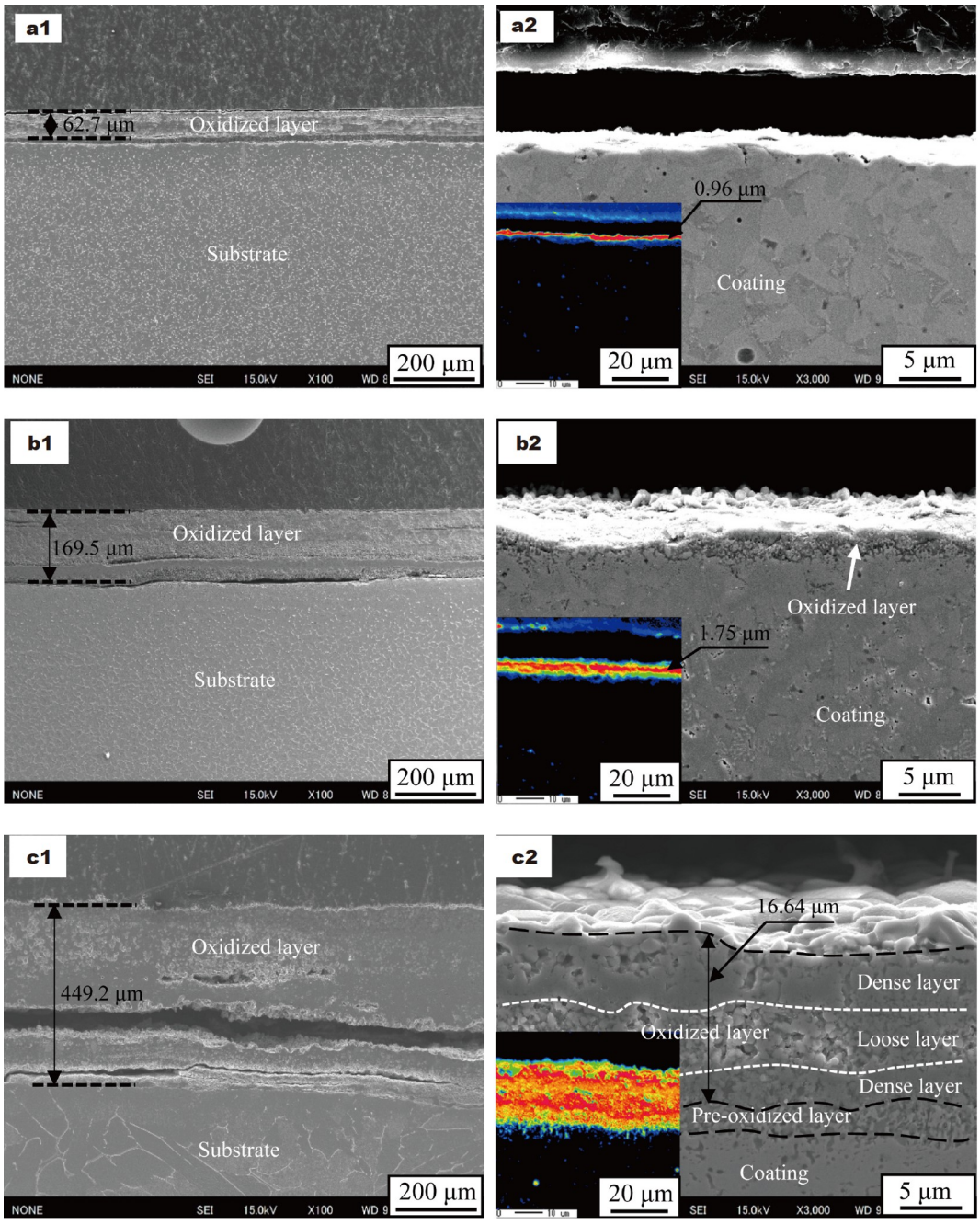

Figure 12 SEM and the corresponding oxygen distribution images at different temperatures. (a1, b1, c1) Ti-6Al-4V at the oxidation temperatures of 800, 900, and 1000°C, and (a2, b2, c2) coating at the oxidation temperatures of 800, 900, and 1000°C. Reprinted with permission from Ref. [130], Copyright 2022, Elsevier.

components of HEAs with hollow sandwich structures, hollow lattice structures, integrated structure realization, and topological structures, thereby realizing lightweight designs and reductions in the overall weights of the components. Meanwhile, excellent performances results can be ensured [137,138]. These are promising application directions in both the aerospace and automobile manufacturing fields.

Graded materials

In industrial fields, different parts of complex components usually play a variety of roles. Therefore, the properties of the required materials will also be different. For example, one position may require materials to possess excellent creep resistance, and another position needs materials to have good corrosion resistance. In other words, connections between a variety of materials may be needed to meet the performance requirements of components [139]. Graded materials are a new type of composite material characterized with continuous gradient changes in compositions and properties achieved by combining two or more types of heterogeneous materials, such as metal/metal, metal/ceramic, metal/non-metal, ceramic/non-metal, and non-metal/plastic combinations [140,141]. SLM technology has

major advantages in the preparation of functionally graded materials [142,143]. For example, it can realize the direct molding of integral components containing a variety of functional materials and provide better dimensional accuracy, while improving the mechanical and functional properties of integral components [144]. Hu *et al.* [145] prepared 316L/CuCrZr functionally graded material with both grain size gradients and dual-scale heterogeneous microstructures using SLM. The unique microstructures ensured that the 316L/CuCrZr graded material combined the advantages of the excellent electrical and thermal conductivity of the CuCrZr alloy and the high strength and hardness of the 316L, which have high application potential in electrical, automotive, and die-casting industries. SLM can not only be used to prepare functional gradient materials, but also in the preparation of compositional gradient materials. Taking equiatomic AlCoCrFeNi and CoCrFeNi powders as feedstock, Guo *et al.* [146] used a customized SLM device to fabricate compositionally graded $Al_xCoCrFeNi$ (x = 0.04–0.75) HEAs, and then investigated the crack problems in detail. The results showed that the chemical segregation of the $Al_xCoCrFeNi$ (x = 0.04–0.75) HEAs promoted the formation of constant dual phase structures. When $x \leq 0.7$, those dual phase structures had effectively inhibited the initiation and propagation of hot tearing problems in metal AM. Similarly, Zhao *et al.* [147] used modified SLM equipment to fabricate CoCrFeNi HEA coupon with stepwise gradation from 0 to approximately 12 at% Ti, in order to ascertain the maximum Ti content that can be added to the HEA for strength enhancement. Subsequently, by observing the cracks of the $CoCrFeNiTi_x$ HEAs, it was determined that a maximum of ~10 at% Ti can be added during SLM.

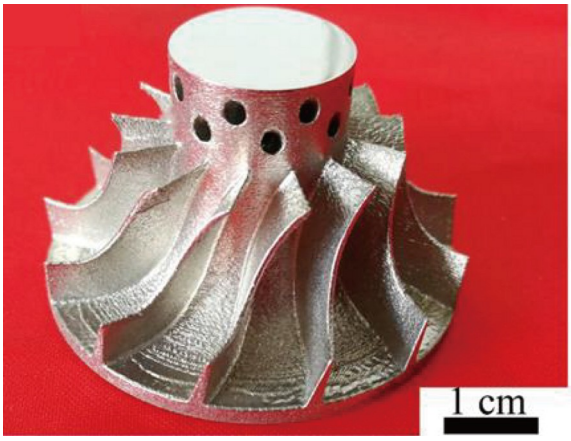

Figure 13 Small turbine blade manufactured *via* SLM. Reprinted with permission from Ref. [34], Copyright 2019, Elsevier.

CONCLUSIONS AND OUTLOOK

As emerging materials, HEAs have many attractive properties due to the huge compositional design space. In recent years, the introduction of SLM technology into HEAs has further broken through the performance advantages of HEAs, and has attracted widespread attention. The HEAs prepared using the SLM technology possess unique microstructures that promote excellent mechanical and functional properties, including cellular sub-

Table 1 Summary of the microstructural characteristics, defects, properties, and applications of SLM-prepared HEAs

Main contents	Features	Constitution/origin/methods of elimination/advantages	Ref.
Microstructural characteristics	Grain morphology	Columnar grains; ultrafine grains	[43–45,48,49]
	Cellular substructures	Composed of many high-density dislocations; derived from the intense heating and cooling of molten pools	[51]
	Precipitates	Intermetallic compounds or oxides	[36,55]
	SFs and nanotwins	Originate from high thermal stress caused by local ultrafast heating and cooling cycles	[58,59]
Defects	Pores Residual stress	Stem from the rapid melting, cooling, and solidification of the molten pools; optimize process parameters; heat treatments	[58,79,88]
	Cracks	Stem from the rapid melting, cooling, and solidification of the molten pools; adjust the compositions of HEAs; optimize process parameters; heat treatments	[36,102,103]
Mechanical properties	Strength and ductility	Greatly improves the strength while maintaining excellent ductility	[104,105]
Functional properties	Magnetic properties	Achieves good combinations of soft magnetic and mechanical properties	[79,119]
	Corrosion resistance	Realizes good combinations of corrosion resistance and mechanical properties	[122,123]
	Oxidation resistance	Exhibits excellent oxidation resistance	[124,126]
Applications	Coating applications	Improves the wear resistance, corrosion resistance, and oxidation resistance of substrate surfaces	[129,130]
	Manufacture of complex components	Produces components with complex shapes by virtue of its high dimensional accuracy and high degree of design freedom	[34,131]
	Graded materials	Realizes the direct molding of integral components containing a variety of functional materials; provides better dimensional accuracy; improves the properties of integral components	[145–147]

structures, precipitates, SFs, and nanotwins. A summary of the microstructural characteristics, defects, properties, and applications of SLM-prepared HEAs is listed in Table 1. However, some defects still remain challenges, such as pores, microscopic cracks, and residual stress. Effective methods for the control of the microstructures and the elimination of the microscopic defects of HEAs, including establishing the internal relationships between the processes, microstructures, and properties, are future research priorities. In addition, the current research reports regarding SLM-processed HEAs have mainly focused on the study of mechanical properties. To date, little research has been conducted regarding the functional materials, such as magnetic materials and energy storage materials. Therefore, considering the present industrial demands for new high-performance functional materials, the development of HEAs that combine excellent mechanical and functional properties through SLM technology should be one of the future development directions.

Received 11 July 2023; accepted 15 August 2023; published online 28 September 2023

1 George EP, Curtin WA, Tasan CC. High entropy alloys: A focused review of mechanical properties and deformation mechanisms. Acta Mater, 2020, 188: 435–474
2 Li K, Chen W. Recent progress in high-entropy alloys for catalysts: Synthesis, applications, and prospects. Mater Today Energy, 2021, 20: 100638
3 Lin KH, Tseng CM, Chueh CC, *et al.* Different lattice distortion effects on the tensile properties of Ni-W dilute solutions and CrFeNi and CoCrFeMnNi concentrated solutions. Acta Mater, 2021, 221: 117399
4 Miracle DB, Senkov ON. A critical review of high entropy alloys and related concepts. Acta Mater, 2017, 122: 448–511
5 Kim DG, Jo YH, Park JM, *et al.* Effects of annealing temperature on microstructures and tensile properties of a single FCC phase Co-CuMnNi high-entropy alloy. J Alloys Compd, 2020, 812: 152111
6 Yan X, Zhang Y. Functional properties and promising applications of high entropy alloys. Scripta Mater, 2020, 187: 188–193
7 Zhang W, Liaw PK, Zhang Y. Science and technology in high-entropy alloys. Sci China Mater, 2018, 61: 2–22
8 Yan X, Zou Y, Zhang Y. Properties and processing technologies of high-entropy alloys. Mater Futures, 2022, 1: 022002
9 Yan X, Liaw PK, Zhang Y. Ultrastrong and ductile BCC high-entropy alloys with low-density *via* dislocation regulation and nanoprecipitates. J Mater Sci Tech, 2022, 110: 109–116
10 Lei Z, Liu X, Wu Y, *et al.* Enhanced strength and ductility in a high-entropy alloy *via* ordered oxygen complexes. Nature, 2018, 563: 546–550
11 Zhang Y, Zhang M, Li D, *et al.* Compositional design of soft magnetic high entropy alloys by minimizing magnetostriction coefficient in $(Fe_{0.3}Co_{0.5}Ni_{0.2})_{100-x}(Al_{1/3}Si_{2/3})_x$ system. Metals, 2019, 9: 382
12 Zuo T, Gao MC, Ouyang L, *et al.* Tailoring magnetic behavior of CoFeMnNiX (X = Al, Cr, Ga, and Sn) high entropy alloys by metal doping. Acta Mater, 2017, 130: 10–18
13 Gorr B, Azim M, Christ HJ, *et al.* Phase equilibria, microstructure, and high temperature oxidation resistance of novel refractory high-entropy alloys. J Alloys Compd, 2015, 624: 270–278
14 Liu YY, Chen Z, Chen YZ, *et al.* Effect of Al content on high temperature oxidation resistance of $Al_xCoCrCuFeNi$ high entropy alloys (x = 0, 0.5, 1, 1.5, 2). Vacuum, 2019, 169: 108837
15 Müller F, Gorr B, Christ HJ, *et al.* On the oxidation mechanism of refractory high entropy alloys. Corrosion Sci, 2019, 159: 108161
16 Zuo T, Cheng Y, Chen P, *et al.* Structural and magnetic transitions of CoFeMnNiAl high-entropy alloys caused by composition and annealing. Intermetallics, 2021, 137: 107298
17 Lee CY, Lin SJ, Yeh JW. (AlCrNbSiTi)N/TiN multilayer films designed by a hybrid coating system combining high-power impulse magnetron sputtering and cathode arc deposition. Surf Coatings Tech, 2023, 468: 129757
18 Sankara Subramanian AT, Meenalochini P, Suba Bala Sathiya S, *et al.* A review on selection of soft magnetic materials for industrial drives. Mater Today-Proc, 2021, 45: 1591–1596
19 Asghari-Rad P, Sathiyamoorthi P, Nguyen NTC, *et al.* A powder-metallurgy-based fabrication route towards achieving high tensile strength with ultra-high ductility in high-entropy alloy. Scripta Mater, 2021, 190: 69–74
20 Peng YB, Zhang W, Mei XL, *et al.* Microstructures and mechanical properties of FeCoCrNi-Mo high entropy alloys prepared by spark plasma sintering and vacuum hot-pressed sintering. Mater Today Commun, 2020, 24: 101009
21 Yue Y, Yan X, Zhang Y. Nano-fiber-structured Cantor alloy films prepared by sputtering. J Mater Res Tech, 2022, 21: 1120–1127
22 Wang M, Lu Y, Lan J, *et al.* Lightweight, ultrastrong and high thermal-stable eutectic high-entropy alloys for elevated-temperature applications. Acta Mater, 2023, 248: 118806
23 Meng A, Chen X, Guo Y, *et al.* Dislocation mediated dynamic tension-compression asymmetry of a $Ni_2CoFeV_{0.5}Mo_{0.2}$ medium entropy alloy. J Mater Sci Tech, 2023, 159: 204–218
24 Jin X, Xue Z, Mao Z, *et al.* Exploring multicomponent eutectic alloys along an univariant eutectic line. Mater Sci Eng-A, 2023, 877: 145136
25 Zhao Q, Sun Q, Xin S, *et al.* High-strength titanium alloys for aerospace engineering applications: A review on melting-forging process. Mater Sci Eng-A, 2022, 845: 143260
26 Ma Y, Sun L, Zhang Y, *et al.* Achieving excellent strength-ductility synergy *via* cold rolling-annealing in Al-containing refractory high-entropy alloys. Int J Refract Met Hard Mater, 2023, 114: 106263
27 Li W, Xiong K, Yang L, *et al.* An ambient ductile TiHfVNbTa refractory high-entropy alloy: Cold rolling, mechanical properties, lattice distortion, and first-principles prediction. Mater Sci Eng-A, 2022, 856: 144046
28 Sun T, Song W, Shan F, *et al.* Phase formation, texture evolutions, and mechanical behaviors of $Al_{0.5}CoCr_{0.8}FeNi_{2.5}V_{0.2}$ high-entropy alloys upon cold rolling. Prog Nat Sci-Mater Int, 2022, 32: 196–205
29 Wang J, Zhou X, Li J, *et al.* A comparative study of Cu–15Ni–8Sn alloy prepared by L-DED and L-PBF: Microstructure and properties. Mater Sci Eng-A, 2022, 840: 142934
30 Wang J, Zhou XL, Li J, *et al.* Microstructures and properties of SLM-manufactured Cu-15Ni-8Sn alloy. Addit Manuf, 2020, 31: 100921
31 Wan X, Lan A, Zhang M, *et al.* Corrosion and passive behavior of $Al_{0.8}CrFeNi_{2.2}$ eutectic high entropy alloy in different media. J Alloys Compd, 2023, 944: 169217
32 Gokcekaya O, Ishimoto T, Hibino S, *et al.* Unique crystallographic texture formation in Inconel 718 by laser powder bed fusion and its effect on mechanical anisotropy. Acta Mater, 2021, 212: 116876
33 Sui Q, Wang Z, Wang J, *et al.* Additive manufacturing of CoCrFeNiMo eutectic high entropy alloy: Microstructure and mechanical properties. J Alloys Compd, 2022, 913: 165239
34 Zhou PF, Xiao DH, Wu Z, *et al.* $Al_{0.5}FeCoCrNi$ high entropy alloy prepared by selective laser melting with gas-atomized pre-alloy powders. Mater Sci Eng-A, 2019, 739: 86–89
35 Fu Z, Yang B, Gan K, *et al.* Improving the hydrogen embrittlement resistance of a selective laser melted high-entropy alloy *via* modifying the cellular structures. Corrosion Sci, 2021, 190: 109695
36 Luo S, Zhao C, Su Y, *et al.* Selective laser melting of dual phase $AlCrCuFeNi_x$ high entropy alloys: Formability, heterogeneous microstructures and deformation mechanisms. Addit Manuf, 2020, 31: 100925
37 Karimi J, Kollo L, Rahmani R, *et al.* Selective laser melting of *in-situ* CoCrFeMnNi high entropy alloy: Effect of remelting. J Manuf Proc, 2022, 84: 55–63
38 Khodashenas H, Mirzadeh H. Post-processing of additively manufactured high-entropy alloys—A review. J Mater Res Tech, 2022, 21: 3795–3814
39 Kamran S, Farid A. Microstructure-tailored stainless steels with high mechanical performance at elevated temperature. In: Zoia D (ed.). Stainless Steels and Alloys. Rijeka: Intechopen Limited. 2018

40 Zhang C, Zhu J, Zheng H, *et al.* A review on microstructures and properties of high entropy alloys manufactured by selective laser melting. Int J Extrem Manuf, 2020, 2: 032003
41 Chen X, Kong J, Feng S, *et al.* A precipitation-strengthened high-entropy alloy prepared by selective laser melting *in-situ* alloying and post-heat treatment. J Alloys Compd, 2023, 936: 168145
42 Kim YK, Baek MS, Yang S, *et al. In-situ* formed oxide enables extraordinary high-cycle fatigue resistance in additively manufactured CoCrFeMnNi high-entropy alloy. Addit Manuf, 2021, 38: 101832
43 Martin JH, Yahata BD, Hundley JM, *et al.* 3D printing of high-strength aluminium alloys. Nature, 2017, 549: 365–369
44 Li Y, Zhou K, Tan P, *et al.* Modeling temperature and residual stress fields in selective laser melting. Int J Mech Sci, 2018, 136: 24–35
45 Cui D, Zhang Y, Liu L, *et al.* Oxygen-assisted spinodal structure achieves 1.5 GPa yield strength in a ductile refractory high-entropy alloy. J Mater Sci Tech, 2023, 157: 11–20
46 Lin D, Xi X, Li X, *et al.* High-temperature mechanical properties of FeCoCrNi high-entropy alloys fabricated *via* selective laser melting. Mater Sci Eng-A, 2022, 832: 142354
47 Chen P, Li S, Zhou Y, *et al.* Fabricating CoCrFeMnNi high entropy alloy *via* selective laser melting *in-situ* alloying. J Mater Sci Tech, 2020, 43: 40–43
48 Lin D, Xu L, Jing H, *et al.* Effects of annealing on the structure and mechanical properties of FeCoCrNi high-entropy alloy fabricated *via* selective laser melting. Addit Manuf, 2020, 32: 101058
49 Li B, Qian B, Xu Y, *et al.* Fine-structured CoCrFeNiMn high-entropy alloy matrix composite with 12 wt% TiN particle reinforcements *via* selective laser melting assisted additive manufacturing. Mater Lett, 2019, 252: 88–91
50 Li B, Zhang L, Xu Y, *et al.* Selective laser melting of CoCrFeNiMn high entropy alloy powder modified with nano-TiN particles for additive manufacturing and strength enhancement: Process, particle behavior and effects. Powder Tech, 2020, 360: 509–521
51 Li Z, Cui Y, Yan W, *et al.* Enhanced strengthening and hardening *via* self-stabilized dislocation network in additively manufactured metals. Mater Today, 2021, 50: 79–88
52 Mu Y, He L, Deng S, *et al.* A high-entropy alloy with dislocation-precipitate skeleton for ultrastrength and ductility. Acta Mater, 2022, 232: 117975
53 Zhu ZG, Nguyen QB, Ng FL, *et al.* Hierarchical microstructure and strengthening mechanisms of a CoCrFeNiMn high entropy alloy additively manufactured by selective laser melting. Scripta Mater, 2018, 154: 20–24
54 Qiu C. A new approach to synthesise high strength nano-oxide dispersion strengthened alloys. J Alloys Compd, 2019, 790: 1023–1033
55 Chen P, Yang C, Li S, *et al. In-situ* alloyed, oxide-dispersion-strengthened CoCrFeMnNi high entropy alloy fabricated *via* laser powder bed fusion. Mater Des, 2020, 194: 108966
56 Zhou R, Liu Y, Liu B, *et al.* Precipitation behavior of selective laser melted $FeCoCrNiC_{0.05}$ high entropy alloy. Intermetallics, 2019, 106: 20–25
57 Lin WC, Chang YJ, Hsu TH, *et al.* Microstructure and tensile property of a precipitation strengthened high entropy alloy processed by selective laser melting and post heat treatment. Addit Manuf, 2020, 36: 101601
58 Li R, Niu P, Yuan T, *et al.* Selective laser melting of an equiatomic CoCrFeMnNi high-entropy alloy: Processability, non-equilibrium microstructure and mechanical property. J Alloys Compd, 2018, 746: 125–134
59 Wu W, Zhou R, Wei B, *et al.* Nanosized precipitates and dislocation networks reinforced C-containing CoCrFeNi high-entropy alloy fabricated by selective laser melting. Mater Charact, 2018, 144: 605–610
60 Chen B, Moon SK, Yao X, *et al.* Strength and strain hardening of a selective laser melted $AlSi_{10}Mg$ alloy. Scripta Mater, 2017, 141: 45–49
61 Tucho WM, Lysne VH, Austbø H, *et al.* Investigation of effects of process parameters on microstructure and hardness of SLM manufactured SS316L. J Alloys Compd, 2018, 740: 910–925
62 Leung CLA, Luczyniec D, Guo E, *et al.* Quantification of interdependent dynamics during laser additive manufacturing using X-ray imaging informed multi-physics and multiphase simulation. Adv Sci, 2022, 9: 2203546
63 Ahmadi M, Tabary SAAB, Rahmatabadi D, *et al.* Review of selective laser melting of magnesium alloys: Advantages, microstructure and mechanical characterizations, defects, challenges, and applications. J Mater Res Tech, 2022, 19: 1537–1562
64 Bonneric M, Brugger C, Saintier N. Investigation of the sensitivity of the fatigue resistance to defect position in aluminium alloys obtained by selective laser melting using artificial defects. Int J Fatigue, 2020, 134: 105505
65 Niu P, Li R, Gan K, *et al.* Microstructure, properties, and metallurgical defects of an equimolar CoCrNi medium entropy alloy additively manufactured by selective laser melting. Metall Mater Trans A, 2021, 52: 753–766
66 Shamsaei N, Yadollahi A, Bian L, *et al.* An overview of direct laser deposition for additive manufacturing; part II: Mechanical behavior, process parameter optimization and control. Addit Manuf, 2015, 8: 12–35
67 Braun J, Kaserer L, Stajkovic J, *et al.* Molybdenum and tungsten manufactured by selective laser melting: Analysis of defect structure and solidification mechanisms. Int J Refract Met Hard Mater, 2019, 84: 104999
68 Jeon JM, Park JM, Yu JH, *et al.* Effects of microstructure and internal defects on mechanical anisotropy and asymmetry of selective laser-melted 316L austenitic stainless steel. Mater Sci Eng-A, 2019, 763: 138152
69 Guan J, Wang Q. The effect of a remelting treatment scanning strategy on the surface morphology, defect reduction mechanism, and mechanical properties of a selective laser-melted Al-based alloy. J Mater Sci, 2022, 57: 9807–9817
70 Dallago M, Winiarski B, Zanini F, *et al.* On the effect of geometrical imperfections and defects on the fatigue strength of cellular lattice structures additively manufactured *via* selective laser melting. Int J Fatigue, 2019, 124: 348–360
71 Peng Y, Jia C, Song L, *et al.* The manufacturing process optimization and the mechanical properties of FeCoCrNi high entropy alloys fabricated by selective laser melting. Intermetallics, 2022, 145: 107557
72 Salem H, Carter LN, Attallah MM, *et al.* Influence of processing parameters on internal porosity and types of defects formed in Ti6Al4V lattice structure fabricated by selective laser melting. Mater Sci Eng-A, 2019, 767: 138387
73 Yang F, Wang L, Wang Z, *et al.* Ultra strong and ductile eutectic high entropy alloy fabricated by selective laser melting. J Mater Sci Tech, 2022, 106: 128–132
74 Balyakin A, Zhuchenko E, Nosova E. Study of heat treatment impact on the surface defects appearance on samples obtained by selective laser melting of Ti-6Al-4V during chemical polishing. Mater Today-Proc, 2019, 19: 2307–2311
75 Wang X, Yu J, Liu J, *et al.* Effect of process parameters on the phase transformation behavior and tensile properties of NiTi shape memory alloys fabricated by selective laser melting. Addit Manuf, 2020, 36: 101545
76 Benedetti M, Santus C. Notch fatigue and crack growth resistance of Ti-6Al-4V ELI additively manufactured *via* selective laser melting: A critical distance approach to defect sensitivity. Int J Fatigue, 2019, 121: 281–292
77 Zhang L, Li Y, Zhang S, *et al.* Selective laser melting of IN738 superalloy with a low Mn + Si content: Effect of energy input on characteristics of molten pool, metallurgical defects, microstructures and mechanical properties. Mater Sci Eng-A, 2021, 826: 141985
78 Ge J, Yuan B, Zhao L, *et al.* Effect of volume energy density on selective laser melting NiTi shape memory alloys: Microstructural evolution, mechanical and functional properties. J Mater Res Tech, 2022, 20: 2872–2888
79 Song X, Liaw PK, Wei Z, *et al.* Evolution of the microstructures, magnetic and mechanical behaviors of $Co_{47.5}Fe_{28.5}Ni_{19}Si_{3.4}Al_{1.6}$ high-entropy alloy fabricated by laser powder bed fusion. Addit Manuf, 2023, 71: 103593
80 Guo Y, Su H, Zhou H, *et al.* Unique strength-ductility balance of

$AlCoCrFeNi_{2.1}$ eutectic high entropy alloy with ultra-fine duplex microstructure prepared by selective laser melting. J Mater Sci Tech, 2022, 111: 298–306
81 Sanaei N, Fatemi A. Defects in additive manufactured metals and their effect on fatigue performance: A state-of-the-art review. Prog Mater Sci, 2021, 117: 100724
82 Gan G, Yang B, Zhang X, *et al.* Tuning the mechanical properties of powder bed fusion printed CoCrFeNiMn high-entropy alloys by annealing and hot isostatic pressing. J Alloys Compd, 2023, 946: 169376
83 Tong Z, Ren X, Jiao J, *et al.* Laser additive manufacturing of FeCrCoMnNi high-entropy alloy: Effect of heat treatment on microstructure, residual stress and mechanical property. J Alloys Compd, 2019, 785: 1144–1159
84 Tong Z, Liu H, Jiao J, *et al.* Microstructure, microhardness and residual stress of laser additive manufactured CoCrFeMnNi high-entropy alloy subjected to laser shock peening. J Mater Proc Tech, 2020, 285: 116806
85 Marola S, Bosia S, Veltro A, *et al.* Residual stresses in additively manufactured AlSi10Mg: Raman spectroscopy and X-ray diffraction analysis. Mater Des, 2021, 202: 109550
86 Ansari P, Salamci MU. On the selective laser melting based additive manufacturing of AlSi10Mg: The process parameter investigation through multiphysics simulation and experimental validation. J Alloys Compd, 2022, 890: 161873
87 Cui X, Zhang S, Zhang CH, *et al.* Additive manufacturing of 24CrNiMo low alloy steel by selective laser melting: Influence of volumetric energy density on densification, microstructure and hardness. Mater Sci Eng-A, 2021, 809: 140957
88 Gu P, Qi T, Chen L, *et al.* Manufacturing and analysis of VNbMoTaW refractory high-entropy alloy fabricated by selective laser melting. Int J Refract Met Hard Mater, 2022, 105: 105834
89 Wang Y, Li R, Niu P, *et al.* Microstructures and properties of equimolar AlCoCrCuFeNi high-entropy alloy additively manufactured by selective laser melting. Intermetallics, 2020, 120: 106746
90 Lin D, Xu L, Jing H, *et al.* A strong, ductile, high-entropy FeCoCrNi alloy with fine grains fabricated *via* additive manufacturing and a single cold deformation and annealing cycle. Addit Manuf, 2020, 36: 101591
91 Zhang M, Zhou X, Wang D, *et al.* AlCoCuFeNi high-entropy alloy with tailored microstructure and outstanding compressive properties fabricated *via* selective laser melting with heat treatment. Mater Sci Eng-A, 2019, 743: 773–784
92 Cain V, Thijs L, Van Humbeeck J, *et al.* Crack propagation and fracture toughness of Ti6Al4V alloy produced by selective laser melting. Addit Manuf, 2015, 5: 68–76
93 Leuders S, Thöne M, Riemer A, *et al.* On the mechanical behaviour of titanium alloy TiAl6V4 manufactured by selective laser melting: Fatigue resistance and crack growth performance. Int J Fatigue, 2013, 48: 300–307
94 Syed AK, Ahmad B, Guo H, *et al.* An experimental study of residual stress and direction-dependence of fatigue crack growth behaviour in as-built and stress-relieved selective-laser-melted Ti6Al4V. Mater Sci Eng-A, 2019, 755: 246–257
95 Li R, Niu P, Yuan T, *et al.* Displacive transformation as pathway to prevent micro-cracks induced by thermal stress in additively manufactured strong and ductile high-entropy alloys. Trans Nonferrous Met Soc China, 2021, 31: 1059–1073
96 Kalentics N, Sohrabi N, Tabasi HG, *et al.* Healing cracks in selective laser melting by 3D laser shock peening. Addit Manuf, 2019, 30: 100881
97 Zheng Y, Zhang K, Liu TT, *et al.* Cracks of alumina ceramics by selective laser melting. Ceramics Int, 2019, 45: 175–184
98 Harrison NJ, Todd I, Mumtaz K. Reduction of micro-cracking in nickel superalloys processed by selective laser melting: A fundamental alloy design approach. Acta Mater, 2015, 94: 59–68
99 Cloots M, Uggowitzer PJ, Wegener K. Investigations on the microstructure and crack formation of IN738LC samples processed by selective laser melting using Gaussian and doughnut profiles. Mater Des, 2016, 89: 770–784
100 Kumar P, Ramamurty U. Microstructural optimization through heat treatment for enhancing the fracture toughness and fatigue crack growth resistance of selective laser melted Ti6Al4V alloy. Acta Mater, 2019, 169: 45–59
101 Zhang C, Feng K, Kokawa H, *et al.* Cracking mechanism and mechanical properties of selective laser melted CoCrFeMnNi high entropy alloy using different scanning strategies. Mater Sci Eng-A, 2020, 789: 139672
102 Sun Z, Tan XP, Descoins M, *et al.* Revealing hot tearing mechanism for an additively manufactured high-entropy alloy *via* selective laser melting. Scripta Mater, 2019, 168: 129–133
103 Miao JW, Wang ML, Zhang AJ, *et al.* Tribological properties and wear mmechanism of $AlCr_{1.3}TiNi_2$ eutectic high-entropy alloy at elevated temperature. Acta Metall Sin, 2023, 59: 267–276
104 Brif Y, Thomas M, Todd I. The use of high-entropy alloys in additive manufacturing. Scripta Mater, 2015, 99: 93–96
105 Lu Y, Wu X, Fu Z, *et al.* Ductile and ultrahigh-strength eutectic high-entropy alloys by large-volume 3D printing. J Mater Sci Tech, 2022, 126: 15–21
106 Wu Y, Zhao X, Chen Q, *et al.* Strengthening and fracture mechanisms of a precipitation hardening high-entropy alloy fabricated by selective laser melting. Virtual Phys Prototyping, 2022, 17: 451–467
107 Chen H, Lu T, Wang Y, *et al.* Laser additive manufacturing of nano-TiC particles reinforced CoCrFeMnNi high-entropy alloy matrix composites with high strength and ductility. Mater Sci Eng-A, 2022, 833: 142512
108 Li R, Kong D, He K, *et al.* Superior thermal stability and strength of additively manufactured CoCrFeMnNi high-entropy alloy *via* NbC decorated sub-micro dislocation cells. Scripta Mater, 2023, 230: 115401
109 Ma Y, Wang Q, Zhou X, *et al.* A novel soft-magnetic B2-based multiprincipal-element alloy with a uniform distribution of coherent body-centered-cubic nanoprecipitates. Adv Mater, 2021, 33: 2006723
110 Vahdati Yekta P, Ghasemi A, Sharifi EM. Magnetic and mechanical properties of cold-rolled permalloy. J Magn Magn Mater, 2018, 468: 155–163
111 Liu C, Peng W, Jiang CS, *et al.* Composition and phase structure dependence of mechanical and magnetic properties for AlCoCuFeNi high entropy alloys. J Mater Sci Tech, 2019, 35: 1175–1183
112 Matsui I, Omura N. Electrodeposition of bulk nanocrystalline Ni–Fe–P alloys and their mechanical and soft magnetic properties. Materialia, 2020, 12: 100766
113 Chaudhary V, Mantri SA, Ramanujan RV, *et al.* Additive manufacturing of magnetic materials. Prog Mater Sci, 2020, 114: 100688
114 Lamichhane TN, Sethuraman L, Dalagan A, *et al.* Additive manufacturing of soft magnets for electrical machines—A review. Mater Today Phys, 2020, 15: 100255
115 Babuska TF, Wilson MA, Johnson KL, *et al.* Achieving high strength and ductility in traditionally brittle soft magnetic intermetallics *via* additive manufacturing. Acta Mater, 2019, 180: 149–157
116 Li S, Lau KB, Wuu D, *et al.* 3D printing of ductile equiatomic Fe-Co alloy for soft magnetic applications. Addit Manuf, 2021, 47: 102291
117 Han L, Maccari F, Souza Filho IR, *et al.* A mechanically strong and ductile soft magnet with extremely low coercivity. Nature, 2022, 608: 310–316
118 Han L, Rao Z, Souza Filho IR, *et al.* Ultrastrong and ductile soft magnetic high-entropy alloys *via* coherent ordered nanoprecipitates. Adv Mater, 2021, 33: 2102139
119 Nartu MSKKY, Jagetia A, Chaudhary V, *et al.* Magnetic and mechanical properties of an additively manufactured equiatomic CoFeNi complex concentrated alloy. Scripta Mater, 2020, 187: 30–36
120 Zhang WR, Liao WB, Liaw PK, *et al.* Effects of transient thermal shock on the microstructures and corrosion properties of a reduced activation high-entropy alloy. J Alloys Compd, 2022, 918: 165762
121 Wang Q, Amar A, Jiang C, *et al.* $CoCrFeNiMo_{0.2}$ high entropy alloy by laser melting deposition: Prospective material for low temperature and corrosion resistant applications. Intermetallics, 2020, 119: 106727
122 Fujieda T, Chen M, Shiratori H, *et al.* Mechanical and corrosion properties of CoCrFeNiTi-based high-entropy alloy additive manu-

factured using selective laser melting. Addit Manuf, 2019, 25: 412–420
123 Thapliyal S, Nene SS, Agrawal P, *et al.* Damage-tolerant, corrosion-resistant high entropy alloy with high strength and ductility by laser powder bed fusion additive manufacturing. Addit Manuf, 2020, 36: 101455
124 Tong Z, Liu H, Jiao J, *et al.* Laser additive manufacturing of CrMnFeCoNi high entropy alloy: Microstructural evolution, high-temperature oxidation behavior and mechanism. Optics Laser Tech, 2020, 130: 106326
125 Jia X, Xu Z, He Y, *et al.* Oxidation behavior of CoCrFeMnNi high-entropy alloy fabricated by selective laser melting. Met Mater Int, 2023, doi: 10.1007/s12540-023-01415-9
126 Chen L, Yang Z, Lu L, *et al.* Effect of TiC on the high-temperature oxidation behavior of WMoTaNbV refractory high entropy alloy fabricated by selective laser melting. Int J Refract Met Hard Mater, 2023, 110: 106027
127 Arif ZU, Khalid MY, ur Rehman E, *et al.* A review on laser cladding of high-entropy alloys, their recent trends and potential applications. J Manuf Proc, 2021, 68: 225–273
128 Karlsson D, Marshal A, Johansson F, *et al.* Elemental segregation in an AlCoCrFeNi high-entropy alloy—A comparison between selective laser melting and induction melting. J Alloys Compd, 2019, 784: 195–203
129 Li D, Chen K, Fu X, *et al.* Effect of WC content on microstructure and properties of CrFeMoNiTi(WC)$_x$ high-entropy alloys composite coatings prepared by selective laser melting. Mater Corrosion, 2022, 73: 1676–1686
130 Li S, Yamaguchi T. High-temperature oxidation behavior of laser-cladded refractory $NiSi_{0.5}CrCoMoNb_{0.75}$ high-entropy coating. J Mater Res Tech, 2022, 17: 1616–1627
131 Ren J, Zhang Y, Zhao D, *et al.* Strong yet ductile nanolamellar high-entropy alloys by additive manufacturing. Nature, 2022, 608: 62–68
132 Plocher J, Panesar A. Review on design and structural optimisation in additive manufacturing: Towards next-generation lightweight structures. Mater Des, 2019, 183: 108164
133 Junk S, Klerch B, Hochberg U. Structural optimization in lightweight design for additive manufacturing. Procedia CIRP, 2019, 84: 277–282
134 Springer H, Baron C, Mostaghimi F, *et al.* Additive manufacturing of high modulus steels: New possibilities for lightweight design. Addit Manuf, 2020, 32: 101033
135 Wang Z, Chen S, Yang S, *et al.* Light-weight refractory high-entropy alloys: A comprehensive review. J Mater Sci Tech, 2023, 151: 41–65
136 Zhang Y, Ai Y, Chen W, *et al.* Preparation and microstructure and properties of AlCuFeMnTiV lightweight high entropy alloy. J Alloys Compd, 2022, 900: 163352
137 Kim YK, Yang S, Lee KA. Superior temperature-dependent mechanical properties and deformation behavior of equiatomic CoCrFeMnNi high-entropy alloy additively manufactured by selective laser melting. Sci Rep, 2020, 10: 8045
138 Cai Y, Li X, Xia H, *et al.* Fabrication of laminated high entropy alloys using differences in laser melting deposition characteristics of FeCoCrNi and FeCoCrNiAl. J Manuf Proc, 2021, 72: 294–308
139 Rodrigues TA, Cipriano Farias FW, Zhang K, *et al.* Wire and arc additive manufacturing of 316L stainless steel/Inconel 625 functionally graded material: Development and characterization. J Mater Res Tech, 2022, 21: 237–251
140 Yan L, Chen Y, Liou F. Additive manufacturing of functionally graded metallic materials using laser metal deposition. Addit Manuf, 2020, 31: 100901
141 Loh GH, Pei E, Harrison D, *et al.* An overview of functionally graded additive manufacturing. Addit Manuf, 2018, 23: 34–44
142 Zhang C, Chen F, Huang Z, *et al.* Additive manufacturing of functionally graded materials: A review. Mater Sci Eng-A, 2019, 764: 138209
143 Zhao S, Zhao Z, Yang Z, *et al.* Functionally graded graphene reinforced composite structures: A review. Eng Struct, 2020, 210: 110339
144 Saleh B, Jiang J, Fathi R, *et al.* 30 Years of functionally graded materials: An overview of manufacturing methods, applications and future challenges. Compos Part B-Eng, 2020, 201: 108376
145 Hu Z, Ma Z, Yu L, *et al.* Functionally graded materials with grain-size gradients and heterogeneous microstructures achieved by additive manufacturing. Scripta Mater, 2023, 226: 115197
146 Guo C, Wei S, Wu Z, *et al.* Effect of dual phase structure induced by chemical segregation on hot tearing reduction in additive manufacturing. Mater Des, 2023, 228: 111847
147 Zhao Y, Lau KB, Teh WH, *et al.* Compositionally graded CoCrFeNiTi high-entropy alloys manufactured by laser powder bed fusion: A combinatorial assessment. J Alloys Compd, 2021, 883: 160825

Acknowledgements This work was supported by Guangdong Basic and Applied Basic Research Foundation (2019B1515120020), the Creative Research Groups of China (51921001), and the National Natural Science Foundation of China (52273280).

Author contributions Song X prepared the manuscript under the direction of Zhang Y. Zhang Y revised the manuscript. All authors contributed to the general discussion.

Conflict of interest The authors declare that they have no conflict of interest.

Xinfang Song is a PhD student under Prof. Zhang's supervision at the State Key Laboratory for Advanced Metals and Materials, University of Science & Technology Beijing (USTB). Her interest focuses on the preparation of high-entropy alloys with high strength and toughness using selective laser melting.

Yong Zhang has been a full professor of the USTB & State Key Laboratory for Advanced Metals and Materials since 2004. He attained his Bachelor degree at Yanshan University in 1991, majored in materials science. He obtained his Master degree majored in nuclear materials in 1993, and PhD degree in composite materials in 1998 at the USTB. Then he worked as a postdoctoral fellow at the Institute of Physics, Chinese Academy of Sciences, and Singapore-Massachusettes Institute of Technology (MIT) Alliance (SMA). His research interest focuses on the study of excellent mechanical and functional properties of high-entropy materials.

激光选区熔化技术制备高熵合金的研究进展

宋鑫芳, 张勇*

摘要 高熵合金的多组分特性使其具有许多传统合金无法比拟的优异性能. 然而, 高熵合金传统的制备方法仍存在一定的局限性. 激光选区熔化(SLM)技术可以通过逐层沉积的方式实现复杂零件的精密成形. 将SLM技术与高熵合金相结合, 可以充分发挥高熵合金的性能优势. 本文综述了SLM制备的高熵合金的显微结构和性能特征. 由于SLM工艺存在高温梯度和高冷却速率, 所以在SLM制备的高熵合金中通常会形成复杂的微观结构, 包括胞状亚结构、析出相、层错和纳米孪晶. 此外, 独特的微观结构为高熵合金带来了优异的力学性能和其他功能, 表明利用SLM技术制备高熵合金具有很大的发展潜力. 此外, 我们还简要介绍了SLM制备的高熵合金的微观缺陷及其应用. 本文为高性能高熵合金的设计提供了有益的指导.

